The interaction between polarized macrophages and fibroblasts in giant cell arteritis

Lessons learned from *in vitro* macrophage skewing and
how to study their effect on fibroblast proliferation and migration

Author	Fokke Walinga
Student number	3823717
Master	Biomedical Sciences
Examiner	P. Heeringa
Project supervisor	W. F. Jiemy
Practical assistors	W. F. Jiemy & S. Xu
Location	University Medical Centre Groningen
Department	Rheumatology and Clinical Immunology
Research group	Vasculitis
Laboratories	EXPIRE, U, Z & REKI
Starting and end date	15-11-2021 to 17-06-2022

ABSTRACT

Giant cell arteritis (GCA) is the most frequent form of vasculitis in older individuals mainly affecting the aorta and extracranial branches of the carotid artery. Vascular lesions are mainly dictated by polarized macrophages (MØs) that are responsible for persistent inflammation, media and elastic lamina degradation, neo-angiogenesis, and intima hyperplasia. Recently, two spatially distributed MØ subsets were discovered associated with tissue destruction and remodeling in GCA lesions. It was proposed that local production of granulocyte macrophage colony-stimulating factor (GM-CSF) skews media resident MØs into $CD206^{+}$, YKL-40^{+}, and IL-6^{high} MØs (GM-MØs), which sequentially prime surrounding MØs with monocyte colony-stimulating factor into FR-β^{+} and PDGF-AA^{high} MØs (M-MØs) located at the adventitia and intima. It is hypothesized that YKL-40 and PDGF-AA are important players in the interaction between GM/M-MØs and fibroblasts in GCA lesions regarding fibroblast proliferation and migration. This crosstalk between GM/M-MØs and fibroblasts can potentially be exploited for GCA-specific markers for diagnosis and treatment. To study this crosstalk, healthy control monocytes were *in vitro* differentiated in the presence of GM/M-CSF into GM/M-MØs and subsequently stimulated with LPS. MØ culture supernatants were acquired and added to cultures of healthy control fibroblasts to study proliferation (MTT assay) and migration (scratch assay). ELISA and qPCR showed no overexpression of CD206, YKL-40, and IL-6 in GM-MØs compared to M-MØ, whereas significantly higher FR-β and PDGF-A expression was shown in M-MØs and GM-MØs, respectively. No differences in fibroblast proliferation and migration were seen between supernatants of GM- and M-MØs. A variety of factors potentially influencing MØ polarization were necessary to accommodate the interaction between MØs and fibroblasts. It was found that the use of a low-glucose concentration in the culture medium strongly influenced the MØ polarization since GM-MØ skewing relies mostly on glucose-dependent metabolic pathways, whereas M-MØ skewing is less glucose dependent. Overall, showing that careful consideration of culture conditions is crucial for *in vitro* approaches of MØ polarization and their effect on fibroblast proliferation and migration.

Keywords: vasculitis, giant cell arteritis, macrophages, granulocyte macrophage colony-stimulating factor, monocyte colony-stimulating factor, fibroblasts

TABLE OF CONTENTS

1. Introduction 3
1.1. Giant cell arteritis 3
1.2. Pathogenesis of GCA 4
1.3. Distinct macrophage subsets in GCA lesions 5
1.4. Potential mediators of vascular remodeling by macrophage subsets in GCA lesions 7
1.5. Outline of the study 8
2. Materials & Methods 9
2.1. Peripheral blood mononuclear cell isolation 9
2.2. Monocyte isolation and macrophage differentiation 9
2.3. Macrophage activation and harvesting 10
2.4. RNA extraction, cDNA synthesis, and qPCR 11
2.5. ELISA 12
2.6. Fibroblast isolation and culturing 13
2.7. MTT assay 13
2.8. Scratch assay 14
2.9. Statistics 15
3. Results 16
3.1. No confirmation of characteristic GM/M-MØ expression pattern 16
3.2. No differential effect of GM/M-MØs on fibroblast migration and proliferation 18
3.3. Undetached MØs show no full restoration of characteristic GM/M-MØ expression pattern 19
4. Discussion 22
4.1. Overview 22
4.2. Possible explanations for uncharacteristic GM/M-MØ expression pattern 22
4.3. Future perspectives 25
5. Conclusion 28
6. References 29
7. Appendix 36
7.1. Optimization of monocyte isolation and macrophage differentiation 36
7.2. Optimization of MTT assay 37
7.3. Optimization of scratch assay 39
7.4. Use of TScratch 40
7.5. Distinct macrophage expression pattern due to GM/M-CSF 41

1. INTRODUCTION

1.1. Giant cell arteritis

Giant cell arteritis (GCA) is an inflammatory disorder of the blood vessels and is most frequently seen in older individuals [1]. GCA affects the medium to large vessels and presents itself as a spectrum of cranial GCA (C-GCA) and large-vessel GCA (LV-GCA) [2]. C-GCA mainly affects the extracranial branches of the carotid artery [3] whilst LV-GCA mostly impacts the aorta and its major branches [4]. It is now increasingly recognized that GCA subtypes can overlap. Depending on the used diagnostic technique, 32 to 83% of patients suffering from C-GCA are also confirmed to have LV-GCA [4,5] whilst 10 to 30% of GCA patients solely suffer from LV-GCA [5]. This illustrates that subtypes of GCA are different presentations of the same disease. Although, GCA affects a variety of medium to large vessels, the most typical presentation is arteritis of the temporal artery (temporal arteritis) [6,7].

The overall prevalence of GCA is around 51 cases per 100,000 individuals annually, but varies a lot between ethnic backgrounds [8]. GCA is almost exclusively seen in individuals over 50 years with a peak incidence at around 75 years of age [9]. GCA is very rare in Africa, Asia, and The Middle East [1], whereas the incidence is much higher in Europa and North and South America [8]. The highest incidence per 100,000 people is observed in Scandinavian countries (21 cases) [8] and in Minnesota, USA (19 cases) [10], which differs significantly from Middle and South Europe (7 cases) [8]. GCA is less seen in individuals of none European origin [10]. Overall, GCA occurs two to three times more often in females compared to males [9]. These epidemiologic findings suggest a role of genetic background in the onset of GCA [1].

Systemic symptoms for GCA comprise fever, weakness, and weight loss as a result of developing chronic inflammation [1]. Specific symptoms for C-GCA include headache, scalp or tongue necrosis, and ischemic complications such as jaw claudication, visual loss, or stroke [1,6,11]. In contrast, LV-GCA patients present with more nonspecific symptoms like fever, but may also display more specific symptoms such as limb claudication or aortic aneurysm and dissection [5,6,11]. When GCA is not treated properly, patients are at risk of occlusion-related ischemia and developing aneurysms due to chronic damage of the vascular wall [12]. Of note, GCA often overlaps with polymyalgia rheumatica (PMR). PMR is characterized by pain and stiffness in the shoulder and neck region accompanied by peripheral arthritis [13]. It has been reported that up to 20% of PMR patients also suffer from GCA [9,13], whereas up to 60% of GCA patients likely have PMR [11,13]. Interestingly, 50% of relapsing GCA patients also show signs of PMR [14].

For many years, the gold standard for GCA diagnosis was a positive temporal artery biopsy (TAB) due to the frequent involvement of the temporal artery [1,15]. The specificity of diagnosis by TAB varies from 81 to 96% [16], though, sensitivity can be as low as 39% [15]. This low sensitivity is due to the segmental and focal nature of the lesions in the vessel wall [17] and the involvement of arteries besides the temporal artery, which is especially seen in LV-GCA [18]. Consequently, there is a risk of a false negative diagnosis by TAB if the biopsy was taken from an unaffected part of the vessel [19]. To overcome these issues, imaging techniques have been increasingly used to aid diagnostics. Ultrasonography (US) or angiography have come in handy for diagnosing C-GCA, whereas computed tomography (CT), magnetic resonance imaging (MRI), positron emission tomography (PET), or a combination of PET and CT have been useful for diagnosing LV-GCA or GCA in general [15,19]. Next to these imaging tools, also assessment of general clinical parameters such as erythrocyte sedimentation rate (ESR) and C-reactive protein (CRP) is used since most patients with GCA show an elevation of these parameters [20].

The main option for GCA treatment remains glucocorticoids (GCs) due to their highly effective and broad suppressive effect on inflammatory cells [6]. Therefore, GCs are often given for over one year to prevent disease relapse. However, this imposes the risk of GC-related complications in almost all patients [21,22]. These complication may comprise hypercortisolism, easy bruising, muscle weakness, bone fractures, or infections [21]. This emphasizes the need of GC-sparing treatments that are specific for GCA lesions. Hence, there is an urgent need for GCA-specific markers to accurately diagnose and precisely treat GCA.

1.2. Pathogenesis of GCA

The etiology of GCA remains obscure but based on many years of research, an immunopathological model of GCA has been proposed [1]. This model is divided into four distinct phases as described below.

Phase 1: Activation of adventitial resident dendritic cells

It all starts with adventitial resident dendritic cells (DCs) of which their toll-like receptors (TLRs) are activated by an unknown trigger causing them to change their phenotype [23,24]. This activation results in high expression of C-C chemokine receptor 7 (CCR7), which traps the DCs in the vessel wall [25]. Next to that, expression of the major histocompatibility complex II (MHC-II) is upregulated, which is important for the activation of T cells [23]. Activated DCs also start to produce cytokines and chemokines. Subsequently, chemokines CCL18, CCL19, CCL20, and CCL21 (chemokine (C-C motif) ligand) recruit $CD4^+$ (positive for cluster of differentiation 4) T cells at the site of inflammation [23,26].

Phase 2: Recruitment, activation, and polarization of $CD4^+$ T cells

The recruited $CD4^+$ T cells infiltrate the vessel wall via the vasa vasorum [26]. In turn, infiltrated T cells are activated and polarized into pro-inflammatory T cell subtypes by the cytokines released by the activated dendritic cells. Activation of these T cells occurs in the presence of pro-inflammatory cytokines IL-12, IL-18, IL-6, IL-1β, and IL-23 (interleukin) and by an unidentified antigen presented by the MHC-II on the DCs [1]. The activated T cells are subsequently polarized into T helper 1 (Th1) cells in the presence of IL-12 and IL-18 [27] or polarized into Th17 cells in the presence of IL-6, IL-1β, and IL-23 [28]. Th1 cells start to produce interferon γ (IFN-γ), whereas Th17 cells mainly release IL-17 [27,28].

Phase 3: Recruitment of $CD8^+$ T cells and monocytes

After the activation and polarization of T cells, $CD8^+$ T cells and especially monocytes are recruited to the site of inflammation. Recruitment of these cells starts with the activation of vascular smooth muscle cells and endothelial cells by pro-inflammatory cytokines released by the polarized T cells [1,29,30]. Subsequently, vascular smooth muscle cells and endothelial cells produce chemokines CCL2, CX3CL1, CXCL9, CXCL10, and CXCL11 (chemokine (C-X-C motif) ligand), which in turn attract the $CD8^+$ cells and monocytes [29]. The chemokines CXCL9, CXCL10 and CXCL11 induce the recruitment of $CXCR3^+$ (positive for chemokine (C-X-C motif) ligand 3 receptor) immune cells, which are mainly $CD8^+$ T cells [31]. These $CD8^+$ T cells release cytotoxic molecules and mainly produce IFN-γ and IL-17, which contribute to the persistent inflammation [31]. Meanwhile, CCL2 and CX3CL1 recruit circulating monocytes expressing CCR2 and CX3CR1 [29,30]. In relation to this, the combination of cytotoxic molecules and IFN-γ also attracts more monocytes to the lesion [31]. These monocytes differentiate into macrophages (MØs) and are further activated by various pro-inflammatory cytokines present in their microenvironment [30]. Some MØs fuse together into more potent multinucleated giant cells (MGCs), which present the pathological hallmark of GCA [29]. Overall, these processes contribute to lesions that are characterized by a granulomatous inflammation of all vessel layers where T cells and MØs constitute the main cell infiltrate [1].

Phase 4: Vascular remodeling by activated macrophages

The last phase of GCA is the chronic and ongoing process of vascular remodeling, mainly dictated by the activated MØs. Activated MØs initiate vessel wall remodeling by their production of cytokines, toxic molecules, and growth factors (GFs) [1,30]. IFN-γ-stimulated monocytes differentiated into MØs are the main source of the cytokines IL-6, IL-1β, and tumor necrosis factor α (TNF-α), which amplify and maintain the local inflammatory response in GCA lesions [32]. MØs activated by IFN-γ produce toxic mediators such as reactive oxygen species (ROS), nitric oxide (NO), and matrix metalloproteinases (MMPs), which cause the destruction of the media and the surrounding elastic lamina [33]. The main MMPs seen in GCA lesions are MMP-2 and MMP-9, whereby MMP-9 is mostly produced by MØs and MGCs closely located to the internal elastic lamina [34]. At last, activated MØs and MGCs produce essentially vascular endothelial GF (VEGF) and platelet-derived GF (PDGF). VEGF induces the formation of new vessels in the media and intima, whereas this is usually restricted to the adventitia only, thereby contributing to more infiltration of immune cells into the vessel wall [35]. On the other hand, PDGF is most likely responsible for the migration and proliferation of tissue resident fibroblasts and vascular smooth muscle cells [36]. These cells migrate to the intima, aided by the destruction of the media and elastic lamina, eventually causing intimal hyperplasia [36]. Altogether, these processes contribute to vascular remodeling and ultimately lead to the occlusion of the affected vessel [9,36].

1.3. Distinct macrophage subsets in GCA lesions

It is clear that MØs play a crucial role in GCA, depicted by their abundance in lesions and their role in inflammation and vascular remodeling. The variety in roles and functions of MØs is due to their incredible plasticity [37]. It is now well established that MØs react to changes in signals from their microenvironment, thereby showing strong heterogeneity in their phenotype and function [38].

Traditionally, MØs were subdivided into classically activated MØs (M1-MØs) or alternatively activated MØs (M2-MØs) [39]. Generally, M1-MØs are considered pro-inflammatory and exhibit strong anti-microbial properties. M1-MØs are classically activated upon stimulation with IFN-γ, lipopolysaccharide (LPS), and granulocyte-macrophage colony-stimulating factor (GM-CSF) and generally express the surface markers CD80, CD86 (both co-stimulatory molecules for T cell activation), and CD64 [40,41]. The pro-inflammatory nature of M1-MØs is illustrated by their secretion of cytokines IL-1β, IL-6, IL-12, IL-23, and TNF-α, whereas their microbicidal abilities are mediated by the production of nitric oxide (NO) and increased phagocytic capabilities. Hence, M1-MØs are also associated with autoimmune diseases like rheumatoid arteritis due to their tissue destructive properties. In contrast, M2-MØs are activated upon the anti-inflammatory cytokines IL-4, IL-10, IL-13, transforming growth factor β (TGF-β), and macrophage CSF (M-CSF) and display more anti-inflammatory and tissue repairing characteristics. Typical M2-MØ surface markers are the macrophage mannose receptor (MMR or CD206) and CD163 [39,40]. With M2-MØs, tissue repair and remodeling are induced by their production of TGF-β and resolution of inflammation is initiated mainly through the production of mainly IL-10 [42]. However, we now know that this *in vitro* based model is an oversimplification of the *in vivo* situation and that it does not recapitulate the complexity of MØ polarization in (inflamed) tissues [43].

Researchers have shifted away from the M1/M2-MØ paradigm towards a new perspective wherein MØs display a mix of both M1- and M2-MØ traits in disease conditions [43]. Nowadays, it is proposed that during disease development distinct MØ subsets exhibit in a spatial and temporal distribution associated with tissue damage and repair [44]. In relation to this, Jiemy et al. (2020) recently identified two spatially distributed MØ subsets associated with tissue destruction and remodeling in GCA lesions [45,46]. The first MØ subtype overexpressed CD206, MMP-9, and chitinase 3-like 1 (YKL-40) and was

mainly found at the media and its borders. This MØ subtype was highly associated with inflammation mainly by IL-6, IL-1β, and TNF-α release, formation of new vessels (neo-angiogenesis), and tissue destruction by degradation of the media and the surrounding elastic lamina. The second MØ subtype was characterized by high expression of the folate receptor β (FR-β) and was found in the intima and adventitia surrounding the other MØ subtype. This MØ subtype was associated with tissue remodeling and intimal hyperplasia, potentially mediated by PDGF-AA and other GFs, which activate fibroblasts. Interestingly, both MØ subsets showed expression of M1- and M2-MØ characteristics.

Regarding the spatially distributed MØ subsets observed in GCA lesions, Jiemy et al. (2020) also discovered the microenvironmental signals likely responsible for the polarization and skewing of the different MØ subsets [45,46]. Local production of a gradient of GM-CSF and M-CSF is suggested to be responsible for the skewing of the two MØ subsets seen in GCA lesions. Earlier, it was already found that GM-CSF and M-CSF are able to cause overexpression of CD206 and FR-β, respectively [40]. In line with this, the study also showed that GM-CSF is produced by infiltrating T cells ($CD4^+$ and $CD8^+$ T cells) at sites of inflammation in GCA and proposed that this local production skews MØs into $CD206^+$, YKL-40^+, and MMP-9^+ MØs (GM-MØs) at the site of the media [45]. Further investigation showed that M-CSF was produced by and localized around GM-MØs, suggesting that this signal skews surrounding MØs in the intima and adventitia into FR-β^+ MØs (M-MØs). Notably, it was also confirmed *in vitro* that GM-CSF and M-CSF skews MØs into the distinct MØs subsets each with their characteristic expression pattern [45]. In summary, it was proposed that within GCA lesions, infiltrating monocytes are sequentially primed by local GM-CSF into tissue destructive GM-MØs, which subsequently release M-CSF that skews surrounding MØs into tissue remodeling M-MØs. [45]. This led to an expansion of the vascular remodeling phase of the pathogenic model of GCA (Figure 1) [46]. Finally, whereas in normal conditions the inflammation is resolved, in GCA it remains. This leads to an amplification of inflammation and tissue remodeling mediated by the distinct MØ subsets, eventually leading to vessel occlusion.

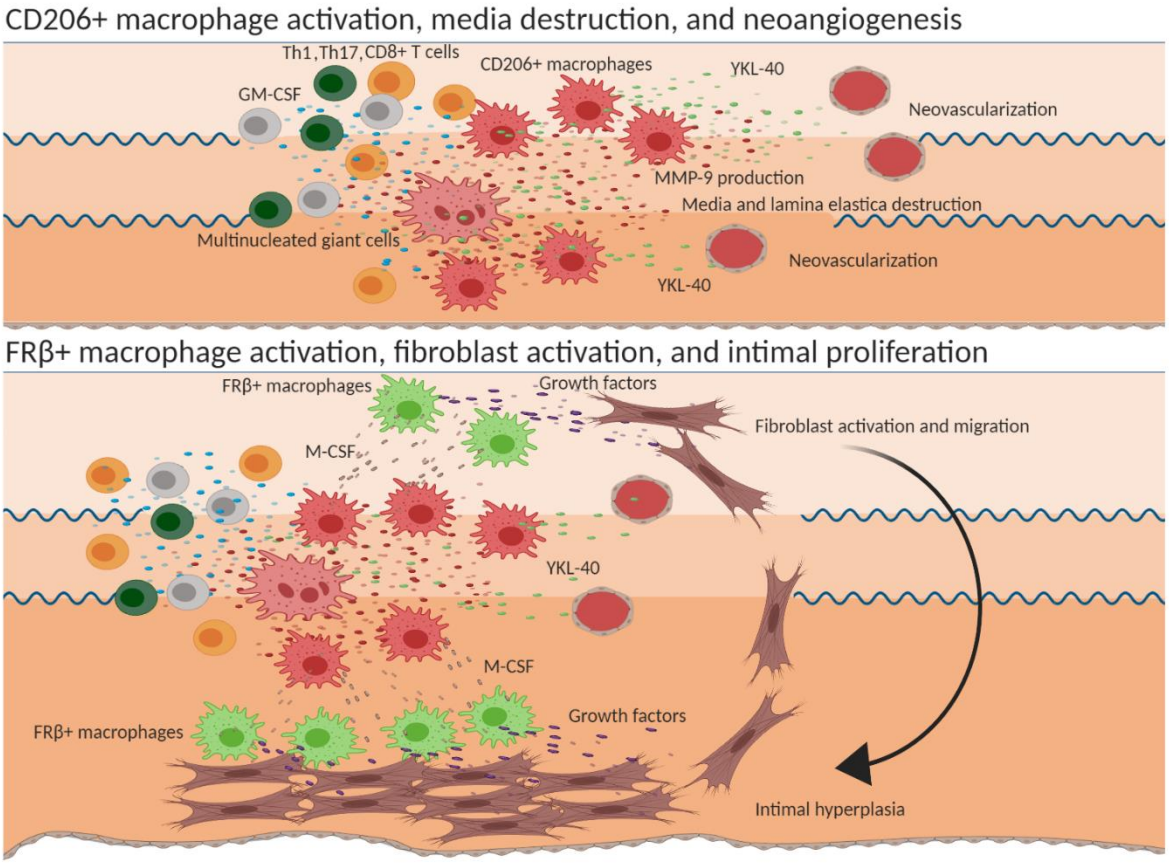

Figure 1. Vascular remodeling in GCA lesions mediated by GM/M-MØs. Initially, GM-CSF released by T cells skews MØs into CD206^{+}, YKL-40^{+}, and MMP-9^{+} MØs responsible for amplification of inflammation, neo-angiogenesis, and media and elastic lamina digestion. Subsequently, M-CSF released by GM-MØs skews surrounding MØs into FR-β^{+} MØs responsible for intimal hyperplasia potentially mediated by PDGF-AA. Ultimately, leading to a loop of inflammation and tissue remodeling mediated by the MØs subsets [46] (Created with BioRender.com).

1.4. Potential mediators of vascular remodeling by macrophage subsets in GCA lesions

The pathologic function of the skewed MØ subsets is linked to the various mediators and factors released by these cells. The growth factors YKL-40 and PDGF-AA are believed to be significant executors of the GM/M-MØs, respectively [45,47].

YKL-40 overexpression by MØs has been reported in various inflammatory pathologies whereby its production was stimulated by GM-CSF and other pro-inflammatory signals [46,48]. As stated previously, it was found in GCA lesions that medial located GM-MØs positive for CD206 express high levels of YKL-40 [45,46]. These GM-MØs are believed to execute their tissue destructive ability due to their overexpression of YKL-40. It was found that YKL-40 induces MMP-9 overexpression in MØs, thereby indirectly contributing to media and elastic lamina degradation [47]. Moreover, YKL-40 showed to be a strong promotor of *in vitro* endothelial tube formation (like neo-angiogenesis) similar to VEGF [47]. Together these processes contribute to T cell infiltration, thus further enhancing inflammation. Furthermore, IL-13Rα2, a confirmed receptor for YKL-40, was highly abundant in infiltrating and residential cells such as leukocytes, MØs, and endothelial cells [46,47]. Collectively, these results highlight the significance and role of YKL-40 in the pathology of GCA.

The role of PDGF-AA as a potent regulator of tissue remodeling has been well established. PDGF-AA was found to be an important inducer of fibroblast proliferation [49]. Interestingly, for asthma, PDGF was found to be essential for myofibroblasts proliferation and migration towards the epithelium [50]. In line with this are the tissue remodeling MØs positive for FR-β and skewed by M-CSF seen in GCA

lesions, which were highly associated with intimal hyperplasia and occlusion severity [45,46]. In regard to M-CSF, M-MØs were also seen to have higher *in vitro* expression of PDGF-AA compared to GM-MØs [45]. Similarly, M-MØs in pulmonary fibrosis also promoted fibroblast proliferation and collagen deposition via PDGF-Rα, a receptor for PDGF-AA [51]. Thus, suggesting that PDGF-AA mediates intimal hyperplasia by enhancing fibroblast proliferation and migration from the adventitia towards the intima. Even so, it may be proposed that fibroblast migration is further aided by YKL-40 due to its role in media and elastic lamina degradation.

The suspected distinct GM/M-MØ subsets seen in GCA lesions together with their potential effectors on fibroblasts are summarized below in Figure 2, representing the main focus of this study.

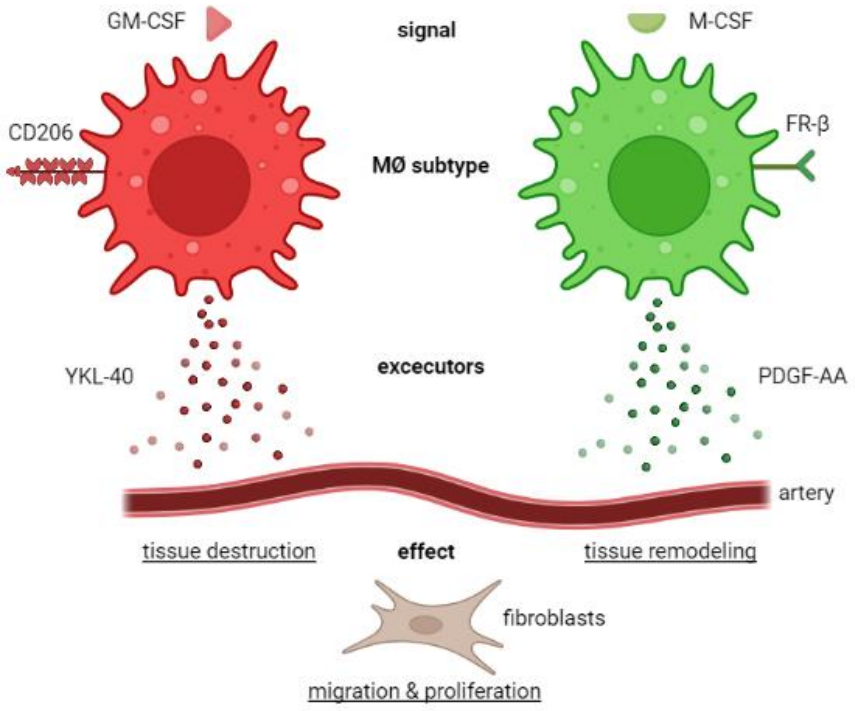

Figure 2. MØ subsets of interest suspected to dictate GCA lesions whereby GM/M-CSF skews MØs into CD206^{+} and YKL40^{high} or FR-β^{+} and PDGF-AA^{high} MØs, respectively (Created with BioRender.com).

1.5. Outline of the study

It is clear that YKL-40 and PDGF-AA are important players in fibroblast proliferation and migration, therefore possibly crucial in the interaction between MØs and their environment in GCA. This crosstalk between MØs and fibroblasts may potentially be exploited for the discovery and development of new disease biomarkers, specific diagnostics, or targeted therapies in GCA. However, knowledge is still limited on the interaction between GM/M-MØs and fibroblasts in GCA and their extent on the proliferative and migratory capacity of fibroblasts. Therefore, this pioneer study aims to elucidate the impact of GM/M-MØs on the proliferation and migration of fibroblasts. To address this issue, monocytes from healthy controls (HCs) are *in vitro* differentiated into MØs in the presence of GM/M-CSF. From this, culture supernatant is taken and added to cultures with HC fibroblasts, which are assessed for their proliferative and migratory capacities using a MTT and scratch assay, respectively. In addition, gene and protein expression of the skewed MØs is determined by qPCR and ELISA. Besides the importance of this research in regard to GCA, also optimization of the MØ culturing and assays is evaluated to further aid future research that deals with the *in vitro* crosstalk between MØs and fibroblasts in GCA or other pathologies.

2. MATERIALS & METHODS

2.1. Peripheral blood mononuclear cell isolation

Peripheral blood mononuclear cells (PBMCs) were isolated from HC buffy coats (6 individuals; named buffy 1-6) or full blood draws (2 individuals; named donor 7-8) using density gradient centrifugation by SepMate™ (StemCell™, Vancouver, Canada). The following procedures were performed sterile in a laminar flow cabinet. Three buffy coat or two blood draw collection tubes were added in a 50 mL tube and topped off to 38 mL with phosphate buffered saline (PBS) (1x). Next, 25 mL of the buffy or blood solution was added down the side of a SepMate™ tube, which was previously filled with 15 mL LymphoPrep™ (StemCell™) (was carefully pipetted through the hole in the bottom). The SepMate™ tubes were centrifuged at 1200 g for 15 minutes with the fastest brake. After centrifugation, SepMate™ tubes were quickly emptied into 50 mL tubes (three SepMate™ tubes per two 50 mL tubes) and topped off to 50 mL with pre-heated RPMI (Roswell Park Memorial Institute; 1640) (Thermo Fisher Scientific, Waltham, MA, USA) (with L-glutamine, 25 mM HEPES, and 1% gentamycin) medium. These 50 mL tubes were centrifuged at 560 g for 8 minutes with the fastest brake. Supernatant was removed and cell pellet was resuspend with 10 mL RPMI per two 50 mL tubes. This cell suspension was counted using the cell counter (Beckman Coulter, Brea, CA, USA) by putting 40 µL cell suspension in 10 mL ISOTON™ II diluent (Beckman Coulter, Brea, CA, USA).

The cell suspension is further processed by adding RPMI to 50 mL followed by centrifugation at 350 g for 8 minutes with the fastest brake. Next, working on ice, supernatant was removed and cell pellet was resuspended with 1 mL RPMI medium (with 20% fetal calf serum (FCS)) per 20 million cells followed by dropwise addition of 1 mL RPMI medium (with 20% dimethyl sulfoxide (DMSO)) per 20 million cells. At last, approximately 10 million of PBMCs in 1 mL of the final cell suspension was added per cryovial. Cryovials with PBMCs were first stored overnight at -80 °C and the next day at -196 °C in liquid nitrogen.

2.2. Monocyte isolation and macrophage differentiation

HC monocytes were isolated from thawed PBMCs using separation based on Percoll® (Cytiva™, Marlborough, MA, USA) gradients followed by culture adherence. This protocol was optimized in the available time span highlighted in Appendix 6.1. The following procedures were performed sterile in a laminar flow cabinet. Starting from day 0, frozen PBMCs were thawed at 37 °C for 10 minutes and transferred to a 15 mL tube in which 9 mL pre-heated (37 °C) regular growth medium (DMEM: Dulbecco's Modified Eagle Medium) (Thermo Fisher Scientific) (1 g/L glucose, 10% FCS, 1% penicillin-streptomycin, and 1% L-glutamine) was added dropwise. The tubes were centrifuged at 300 g for 5 minutes. The cell pellet was resuspend in 1 mL 60% standard isotone Percoll® (SIP: 10x PBS (13.5 g NaCl, 0.1 g Na_2HPO_4, and 2.1 g KH_2PO_4 in 200 mL demi water, filter sterilized, pH 4.6) mixed with Percoll® solution in 1:9 ratio) (SIP is diluted with DMEM with 1% FCS) per PBMC cryovial. The cell suspension in 60% SIP was layered per 2 mL with 4.5 mL 47.5% SIP followed by 2 mL 34% SIP in a regular 15 mL tube. The tubes were centrifuged at 1750 g for 45 minutes with slow acceleration and no brake. After centrifugation, monocytes were harvested by taking the upper interface of the gradients. Cell suspensions of the same donor were pooled and subsequently washed twice with DMEM (1% FCS) (with first wash added to 45 mL and with second wash added to 20 mL) followed by centrifugation at 300 g for 5 minutes (before the second wash, 1 mL of cell suspension was counted using 10 µL in a hemacytometer). Depending on the cell count, cell pellets were resuspended with either 1 or 0.5 mL regular growth medium per PBMC cryovial and respectively seeded in a 12 or 24 well plate with 1 or 0.5 mL per well (used 1 mL for > 0.75 million cells per cryovial and 0.5 mL for < 0.75 cells per cryovial). This difference in protocol was to maintain a constant and appropriate cell density in the monocyte

culture during the MØ differentiation. For the monocyte isolations of PBMCs from buffy 1-6, over 0.75 million cells were obtained, whereas for donor 7-8 under 0.75 million cells were obtained per cryovial.

Following the isolation based on Percoll® gradients, cells were incubated for 4 hours at 37 °C and 5% CO_2 to allow monocyte adherence. After 4 hours, the monocyte culture was carefully washed twice with 1 mL DMEM followed by addition of 50 ng/mL GM-CSF or M-CSF (Peprotech, Rocky Hill, CT, USA) in 1 or 0.5 mL regular growth medium. Over the course of 7 days, monocytes were differentiated into skewed MØs in the presence of the growth factors. Medium plus factors were replaced on days 3 and 5 whereby culture supernatant was spun down (300 g for 5 minutes), and cell pellet was resuspended with medium containing factors and subsequently added to the monocyte culture.

2.3. Macrophage activation and harvesting

The MØs skewed by GM-CSF and M-CSF (also noted as GM- and M-MØs or GM/M-MØs) isolated from buffy 1-6 were detached and activated in a normalized cell number, whereas the remaining GM/M-MØs isolated from donor 7-8 were activated on day 7 without detaching and thus without normalizing the cell number. The difference in protocol was due to the availability of stored PBMCs and had nothing to do with the origin of the PBMCs. The following procedures were performed sterile in a laminar flow cabinet.

On day 7, MØs isolated from buffy 1-6 were detached with 1 mL pre-heated (37 °C) TrypLE™ Express Enzyme (Gibco™, Waltham, MA, USA) for a minimum of 10 minutes at 37 °C and 5% CO_2 followed by addition of 2 mL regular growth medium to inactivate the enzyme. The cell suspension was centrifuged at 300 g for 5 minutes whereafter the cell pellet was resuspended in 1 mL regular growth medium and counted using a hemacytometer. MØ activation was performed preferably at 100,000 cells/mL in 1 mL per well in a 24 well plate with (un)stimulated conditions per GM/M-MØs. Though, depending on the total amount of cells per condition, MØ activation could also be performed with 50,000 cells in 0.5 mL per well in a 48 well plate also with (un)stimulated conditions. Activation was done in the presence of 50 ng/mL GM/M-CSF with or without 100 ng/mL LPS for a period of 4 hours at 37 °C and 5% CO_2. After 4 hours, the new MØ culture was washed twice with either 2 or 1 mL regular growth medium to get rid of the factors and stimulant, and either 1 or 0.5 mL fresh regular growth medium was added. If some cells did not adhere properly, culture supernatant was spun down (300 g for 5 minutes), and cell pellet was resuspended with regular growth medium and added to the MØ culture. The (un)activated MØs were subsequently incubated for 24 hours at 37 °C and 5% CO_2 to let them release their soluble factors in the culture supernatant. After 24 hours, supernatants were collected and spun down at 300 g for 5 minutes followed by taking the acquired supernatant, which was stored at -20 °C for later use (ELISA, MTT assay, and scratch assay). The remaining cell pellet was lysed together with the lysate solution described next. MØs were lysed with buffer RLT (Qiagen, Hilden, Germany) with 1% β-mercaptoethanol using 75 µL for under 100,000 cells and 350 µL for over 100,000 cells. Cell lysates were stored at -80 °C for later use (RNA extraction).

For MØs isolated from donor 7-8, activation was performed on day 7 similarly as MØs isolated from buffy 1-6, but without detaching. In this case, all MØs cultures were activated for 4 hours followed by addition of regular growth medium with or without 50 ng/mL GM/M-CSF. After similar obtainment of supernatants after the 24 hours of incubation, MØs were detached and counted similarly as with MØs isolated from buffy 1-6. Counting was performed to normalize ELISA results so that these are comparable with results from the MØ activation at a normalized cell number. Thereafter, cell suspension was spun down (300 g for 5 minutes) whereafter the cell pellet was lysed similarly as with the MØs isolated from buffy 1-6.

Monocyte isolation and macrophage differentiation (Materials & Methods 2.2), activation, and harvesting (Materials & Methods 2.3) of MØs isolated from buffy 1-6 (buffy coat PBMCs) or donor 7-8 (blood draw PBMCs) are summarized below in Figure 3.

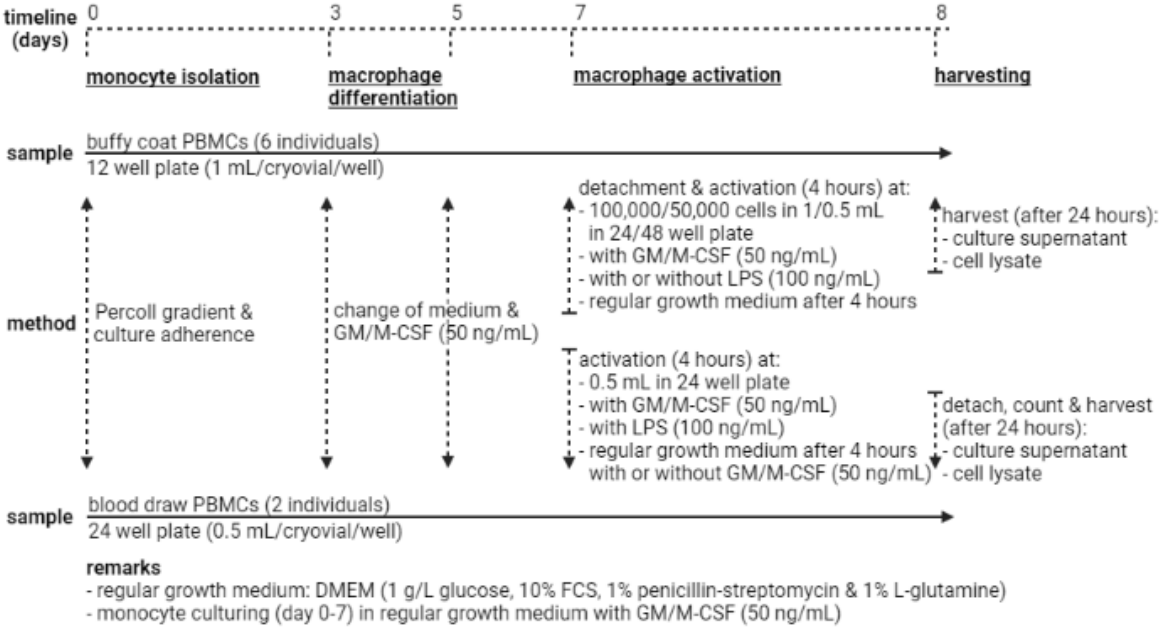

Figure 3. Timeline of monocyte isolation and macrophage differentiation, activation, and harvesting (Created with BioRender.com).

2.4. RNA extraction, cDNA synthesis, and qPCR

Total RNA was extracted from GM/M-MØ lysates using the RNeasy® Micro Kit (Qiagen) according to the following protocol. Per sample, cell lysate was homogenized with 70% ethanol in a 1:1 ratio and transferred to an RNeasy MinElute® spin column with a 2 mL collection tube, which was centrifuged for 30 seconds at maximum g. Flow-through of the collection tube was discarded and 350 µL buffer RW1 was added to the spin column, which was centrifuged for 30 seconds at maximum g. Again, flow-through was discarded and 10 µL DNase I together with 70 µL buffer RDD was added to the center of the spin column. Spin columns were incubated for 15 minutes at room temperature followed by addition of 350 µL buffer RW1. Spin columns were subsequently centrifuged for 30 seconds at maximum g whereafter the columns were placed in new collection tubes. Following, 500 µL buffer RPE was added to the spin column, which was centrifuged for 30 seconds at maximum g. Again, the spin column was placed in a new collection tube followed by addition of 500 µL 80% ethanol to the spin column. Spin columns were centrifuged for 2 minutes at maximum g whereafter the spin column was placed in a new collection tube. Spin columns were centrifuged for 5 minutes at maximum g with open lid to dry the membrane. At last, spin columns were placed in 1.5 mL collection tubes and 15 µL RNase-free water was added directly to the center of the column membrane followed by incubation for 2 minutes at room temperature and centrifugation for 1 minute at maximum g to elute the RNA. From this point onwards, RNA was kept on ice. RNA concentration was determined using a NanoPhotometer (Implen, Munich, Germany).

The extracted RNA was reverse transcribed into cDNA using Superscript III reverse transcriptase (RT) (Invitrogen, Waltham, MA, USA) according to the following protocol. Enzymes, other factors, and mixtures were vortexed and spun down before use or after composing. Per sample, 0.5 µL random hexamers (250 mM) (Promega, Madison, WI, USA) together with 1 µL dNTP mix (10 mM) (Fermentas, Waltham, MA, USA) was prepared as master mix I and added to 12 µL RNA extract in a 0.2 mL tube.

This mixture was heated at 65 °C for 5 minutes followed by 4 °C at infinite minutes in a thermocycler (MyCycler™) (Bio-Rad, Hercules, CA, USA). Thereafter, per sample, 4 μL first strand buffer (5x), 1 μL DTT, 1 μL RNase OUT inhibitor (40 units/μL), and 0.5 μL Superscript III RT (200 units/μL) was combined as master mix II, which was added to the 0.2 mL tubes. This mixture was heated to 25 °C for 5 minutes, 50 °C for 60 minutes, 70 °C for 15 minutes, and cooled to 4 °C at infinite minutes in the thermocycler. The resulting mixture contained the converted cDNA, which was diluted to 10 ng/mL with RNase-free water for qPCR (assumed was that RNA converted 1:1 to cDNA). The cDNA was stored at -20 °C until further use.

Real-time qPCR was carried out using a ViiA™ 7 Real-Time PCR System with TaqMan™ (Thermo Fisher Scientific) primer probes targeting β-actin, CD206, FR-β, YKL-40, PDGF-A, and IL-6 (control for GM-MØs) (details listed below in Table 1) according to the following protocol. For each gene and condition, triplicates were carried out. For samples buffy 3 and 4 with unstimulated GM-MØs, not enough cDNA was obtained to perform triplicates for the genes CD206, FR-β, YKL-40, and PDGF-A, so instead duplicates or singlets were carried out, respectively. As for IL-6, not enough cDNA of buffy 3 and 4 with unstimulated GM-MØs was available to perform qPCR and for buffy 3 with unstimulated M-MØs only duplicates were carried out. To start, 1 μL of cDNA solution (10 ng cDNA) was put per sample in a 384 well plate meant for qPCR. The cDNA solution was subsequently dried for 1 hour with a SpeedVac™ (Thermo Fisher Scientific) ran with the standard procedure. Afterwards, per well, 10 μL of qPCR master mix (0.5 μL Primer Probe Mix (20x), 4.5 μL Milli-Q water, and 5.0 μL ABsolute qPCR ROX Mix (Thermo Fisher Scientific)) was added to the corresponding well and to a well for the no template control (NTC). The 384 well plate was sealed with an optical seal and centrifuged shortly. For the real-time qPCR, hold stage was carried out at 95 °C for 15 minutes followed by the PCR stage, which cycled 45 times from 95 °C for 15 seconds to 60 °C for 1 minute. PCR results were analyzed using QuantStudio™ Real-Time PCR software v1.3 (Applied Biosystems®, Waltham, MA, USA) where relative gene expression was normalized to β-actin as an internal control.

Table 1. Details of primer probes used for real-time qPCR

Gene	Full or alternative name	Gene ID	Probe ID
β-actin	Beta-actin	ACTB	Hs99999903_m1
CD206	Mannose receptor	MRC1	Hs00267207_m1
FR-β	Folate receptor beta	FOLR2	Hs00265255_m1
YKL-40	Chitinase-3-like protein 1	CHI3L1	Hs01072228_m1
PDGF-A	Platelet-derived growth factor A	PDGFA	Hs00964426_m1
IL-6	Interleukin 6	IL6	Hs00174131_m1

2.5. ELISA

YKL-40, PDGF-AA, and IL-6 concentrations of culture supernatants from GM/M-MØs were determined using the human chitinase 3-like 1 (YKL-40), PDGF-AA, and IL-6 DuoSet ELISA (DY-2599, DY-221, and DY206, respectively) (R&D Systems, Minneapolis, MN, USA) according to the following protocol. All incubation steps were done with a sealed plate at an EASIA shaker at room temperature. The washing procedure was standard by washing 5 times with 100 μL wash buffer (0.025 M Tris, 0.15 M NaCl, and 0.05% Tween-20) at a microplate washer. Costar™ (Corning Incorporated, Corning, NY, USA) EIA plates were coated per well with reconstitute lyophilized capture antibody in 100 μL PBS (1x) (2 μg/mL for YKL-40, PDGF-AA, and IL-6) and incubated overnight followed by washing. Thereafter, 200 μL block buffer (PBS (1x) with 2% bovine serum albumin (BSA)) was added to the plate, which was incubated for 1 hour followed by washing.

For the plate setup, standard curves were done in duplicate with two-fold dilutions starting from 2000 to 15.6 pg/mL for YKL-40, 1000 to 7.8 pg/mL for PDGF-AA, and 600 to 4.7 pg/mL for IL-6 of reconstitute lyophilized recombinant protein. Samples were also executed in duplicate with dilutions 1:800 for YKL-40, 1:2 for PDGF-AA, and 1:60 for IL-6. Reagents were diluted in incubation buffer (PBS (1x) with 1% BSA) whereby 100 µL solution was added to the plate, which was incubated for 2 hours. Following subsequent washing, 100 µL incubation buffer with reconstitute lyophilized detection antibody (200 ng/mL for YKL-40, 1 µg/mL for PDGF-AA, and 50 ng/mL for IL-6) was added to the plate, which was incubated for 1 hour followed by washing. Thereafter, 100 µL incubation buffer with streptavidin poly-HRP (horseradish-peroxidase) (Sanquin, Amsterdam, Netherlands) (diluted 1:8000) was added to the plate, which was incubated for 1 hour followed by washing. For the following chromogen reaction, 2 TMB (3,3', 5,5'-tetramethylbenzidine) pills (Sigma-Aldrich, Saint Louis, MO, USA) were dissolved in 11 mL reaction buffer (0.1 M acetate buffer, pH 6.0) wherein 2 µL of 30% H_2O_2 was added just before use. From this solution, 100 µL was added to the plate to start the reaction (incubated), which was stopped when the color of the lowest point of the standard curve became above the blank by adding 100 µl 2N H_2SO_4 (shortly incubated). Absorbance was measured at 450 with a reference filter at 575 nm using a microplate reader (VersaMax™) (Molecular Devices, San Jose, CA, USA). Protein concentration of the supernatant was calculated using the 5 parameter logistic curve-fit that was applied to the absorbances and known protein concentrations of the standard curve. Values below the detection limit of the lowest point of the standard curve were assigned 0 ng or pg/mL.

2.6. Fibroblast isolation and culturing

HC fibroblasts were isolated from a skin breast biopsy of a 65 year old woman. The following procedures were performed sterile in a laminar flow cabinet. Isolation was done by incubating (37 °C and 5% CO_2) small tissue pieces with Ham's F-12 mixed with amnioMAX™ (Thermo Fisher Scientific) (mixed in 3:2 ratio and supplemented with 10% FCS and 1% penicillin-streptomycin) for two weeks in a 6 well plate, while changing medium every two to three days. In this time, fibroblasts grew out of the tissue pieces. These fibroblasts were subsequently isolated from keratinocytes based on digestion time (fibroblasts needed 2 minutes digestion time whereas keratinocytes needed minimally 5 minutes) using 0.05% trypsin-EDTA (filter-sterilized trypsin with EDTA (20 mg per 100 mL) diluted in PBS (1x)).

Next, fibroblasts were cultured at 37 °C and 5% CO_2 in a T25 flask with 5 mL regular growth medium. After reaching 80-100% confluency, fibroblasts were passaged into one T75 flask by washing twice with 3 mL DMEM followed by digestion using 0.05% trypsin-EDTA for 3 minutes. Afterwards, trypsin-EDTA was aspirated and cells were tapped loose followed by resuspending of the cells with 3 mL regular growth medium. This cell suspension was added into the T75 flask together with 12 mL regular growth medium. This fibroblast culture was subsequently passaged at 80-100% confluency (approximately every week) 1 to 2 into new T75 flasks with a similar procedure, but instead, washing was with 7 mL DMEM and resuspending was with 6 mL regular growth medium.

2.7. MTT assay

To assess the proliferative capacity of fibroblasts in the presence of MØ culture supernatant from buffy 1-6, a MTT assay is conducted as an indicator for cell amount. This protocol was optimized in the available time span highlighted in Appendix 6.2. The following procedures were performed sterile in a laminar flow cabinet. Fibroblasts were obtained from 80-100% confluent fibroblast cultures in T75 flasks (passage 4) by detaching with 0.05% trypsin-EDTA (similar as with fibroblast culturing in Materials & Methods 2.6). The obtained cell suspension was centrifuged (300 g for 5 minutes) whereby the cell pellet was resuspended with 3 mL low-serum growth medium (DMEM with 0.1% FCS, 1% penicillin-streptomycin, and 1% L-glutamine). From here, a cell concentration of 50,000 cells/mL in

low-serum growth medium was prepared by counting the cell suspension with a hemacytometer. Thereafter, 5,000 cells in 100 µL low-serum growth medium were seeded per well in a 96 well plate and incubated for 24 hours at 37 °C and 5% CO_2. Also 100 µL low-serum growth medium without cells was seeded to serve as a plate blank.

Following incubation, 50 µL culture medium was removed and 50 µL of corresponding MØ culture supernatant (thawed at room temperature and shortly vortexed) was added to establish a supernatant concentration of 50%. As for the negative control, 50 µL low-serum growth medium was added, whereas for the positive control, 50 µL low-serum growth medium with 100 ng/mL transforming growth factor-β (TGF-β) (final concentration is 50 ng/mL) was added. All conditions, controls, and plate blank were carried out in triplicate. The following fibroblast culture was incubated over a course of 3 days. Thereafter, 10 µL MTT solution (MTT (3-(4,5-dimethylthiazol-2-yl)-2,5-diphenyltetrazolium bromide) dissolved in regular growth medium at 5 mg/mL and filter-sterilized) was added to each well and the culture was incubated for 3 hours at 37 °C and 5% CO_2. At last, medium was discarded and 100 µL solvent (DMSO and ethanol in 1:1 ratio) was added followed by shaking on an orbital shaker for 15 minutes to dissolve the formed formazan crystals. Absorbance was measured at 570 nm using a microplate reader (Molecular Devices) of which the absorbance of the plate blank was subtracted. The final absorbance is proportional to the cell number and thus an indicator for fibroblast proliferation. Proliferative capacity is represented as the fold change of the absorbance of the conditions compared to the absorbance of the negative control.

2.8. Scratch assay

Fibroblast migration was monitored using a scratch assay to assess the migratory capacity of fibroblasts in the presence of MØ culture supernatant from buffy 1-6. This protocol was optimized in the available time span highlighted in Appendix 6.3. The following procedures were performed sterile in a laminar flow cabinet. Fibroblasts were obtained similarly as with the MTT assay in Materials & Methods 2.7 (also passage 4). Following that, 50,000 cells in 500 µL low-serum growth medium were seeded per well in a 24 well plate and incubated for 24 hours at 37 °C and 5% CO_2 so that a cell monolayer was established. After incubation, the monolayer was scratched in a cross using a p1000 pipet tip on a micropipette and a straight ruler. The culture was washed twice with 1 mL DMEM followed by addition of 450 µL low-serum growth medium and 50 µL corresponding culture supernatant (thawed at room temperature and shortly vortexed) to establish a supernatant concentration of 10%. As for the negative control, 50 µL low-serum growth medium was added, whereas for the positive control, 50 µL low-serum growth medium with 500 ng/mL TGF-β (final concentration is 50 ng/mL) was added. All conditions and controls were carried out as a singlet.

The fibroblast culture was incubated at 37 °C and 5% CO_2 and four images (100x magnification) per condition were taken at 0, 16, and 24 hours post-scratch using an inverted microscope (Leica DM IL LED) (Leica Microsystems, Wetzlar, Germany) connected to a computer screen. Migration was quantified using TScratch (available from CSE-lab, Zurich, Switzerland) with the obtained pictures. For TScratch, the standard analysis and advanced settings were used (default threshold 0.25, disk radius 7, minimum whole area and island 0.07, and erosion size 2). During TScratch analysis, images were first globally analyzed in the group editing mode. Additionally, each image got reviewed in single image mode to correctly identify the open wound area using the general threshold slider (algorithm for open image area) and the paint tool (highlighted in Appendix 6.4). If necessary, images were excluded when no proper analysis could be made. Fibroblast migration is expressed as migration area (%) = $((A_0 - A_n)/A_0) \times 100\%$, where A_0 is the initial open area and A_n is the open area at time of measurement.

Migratory capacity is represented as the fold change of migration area (%) of the conditions compared to migration area (%) of the negative control.

2.9. Statistics

Data were analyzed using GraphPad Prism (Version 9.0.0, GraphPad Software, San Diego, CA, USA). For the data from buffy 1-6 of (un)stimulated GM/M-MØs, normal (Gaussian) distribution of the data was assessed by using a Kolmogorov-Smirnov normality test. If the data was normally distributed, differences were assessed using a matched one-way ANOVA (parametric) test. If the data was not normally distributed or when the sample size was too low to test distribution, an unmatched one-way ANOVA (Kruskal Wallis) was performed. For the data from donor 7-8 of stimulated GM/M-MØs, no statistics were performed due to the low sample size. Statistical differences between conditions with a p-value below 0.05 were considered significant. ANOVA significance was indicated on top of the figure, whereas differences for ANOVA post hoc analysis were indicated between groups with ns (not significant; $p > 0.5$), $*$ ($p < 0.5$), $**$ ($p < 0.01$), and $***$ ($p < 0.001$). For buffy 1-6 and donor 7-8 of (un)stimulated GM/M-MØs, data is represented in scatter plots with bar (colored per sample) or connected plots (for unstimulated or stimulated GM/M-MØs). For data from buffy 1-6, median plus interquartile range is showed, whereas with data from donor 7-8, data is represented with the mean plus standard deviation.

Noteworthy, all data from buffy 4 were excluded from analysis for the following reasons. For qPCR analysis, it was observed that the data of unstimulated GM-MØs from buffy 4 contained unexpected high values for various measurements. Using the ROUT method in GraphPad Prism, outliers were identified for qPCR data of CD206, YKL-40, FR-β, and PDGF-A of unstimulated GM-MØs and ELISA data of YKL-40 of unstimulated and stimulated M-MØs from buffy 4. Based on this, we decided to exclude all measurements related to buffy 4 (qPCR, ELISA, scratch assay, and MTT assay). Besides, for qPCR analysis of IL-6, data was also excluded for MØs from buffy 3 since the amount of cDNA from unstimulated GM-MØs was insufficient. However, because IL-6 served as a control for the GM-MØs, this had no further impact on the overall analysis of the data.

3. RESULTS

3.1. No confirmation of characteristic GM/M-MØ expression pattern

The crosstalk between MØs and fibroblasts was studied by assessing the effect of unstimulated and stimulated GM/M-MØ culture supernatant in a fibroblast proliferation and migration assay. To confirm the skewing of MØs into GM/M-MØs with their proposed characteristics, qPCR and ELISA were performed targeting CD206, YKL-40, IL-6, FR-β, and PDGF-A(A). The following describes the qPCR and ELISA results of detached GM/M-MØs that were unstimulated and stimulated at a normalized cell number.

On the mRNA level, no distinct CD206, YKL-40, and IL-6 expression pattern was seen between GM-MØs and M-MØs of both unstimulated and stimulated MØ subtypes (Figure 4-A/B/C). Interestingly, significant differences were seen for YKL-40 expression between unstimulated and stimulated GM/M-MØs with higher expression in LPS stimulated MØs (Figure 4-B2). At the protein level, also no difference in YKL-40 and IL-6 production was seen between GM-MØs and M-MØs of both unstimulated and stimulated MØ subsets (Figure 5-A/B). Again, it was confirmed that LPS stimulation increases YKL-40 and especially IL-6 protein levels (Figure 5-A1/B1), with no detected IL-6 protein in unstimulated MØs. Generally, it was found that YKL-40 levels are much higher compared to CD206 and IL-6 levels, indicated by the relative mRNA expression and protein concentration (Figure 4-B1 and Figure 5-A1). Altogether, these results did not confirm the typical phenotypic characteristics of GM-MØs ($CD206^{+}$, $YKL\text{-}40^{+}$, and $IL\text{-}6^{high}$) previously reported [45,47].

For FR-β mRNA expression, a distinct pattern was observed between the different MØ conditions. Compared to unstimulated and stimulated GM-MØs, a significant higher FR-β expression was seen in unstimulated M-MØs and a trend towards higher expression was seen in stimulated M-MØs (Figure 4-D). In contrast, minimal expression of FR-β was seen in GM-MØs. For the expression of PDGF-A, a significant increase was seen for GM-MØs compared to M-MØs for both unstimulated and stimulated MØ subsets (Figure 4-E). However, relative PDGF-A expression was very low compared to the other genes tested. For PDGF-AA protein levels, no significant differences were seen between MØ conditions (Figure 5-C). Overall, these results confirmed the typical FR-β expression in M-MØs reported previously [45]. In contrast to previous reports, higher PDGF-A mRNA levels were seen in GM-MØs [45].

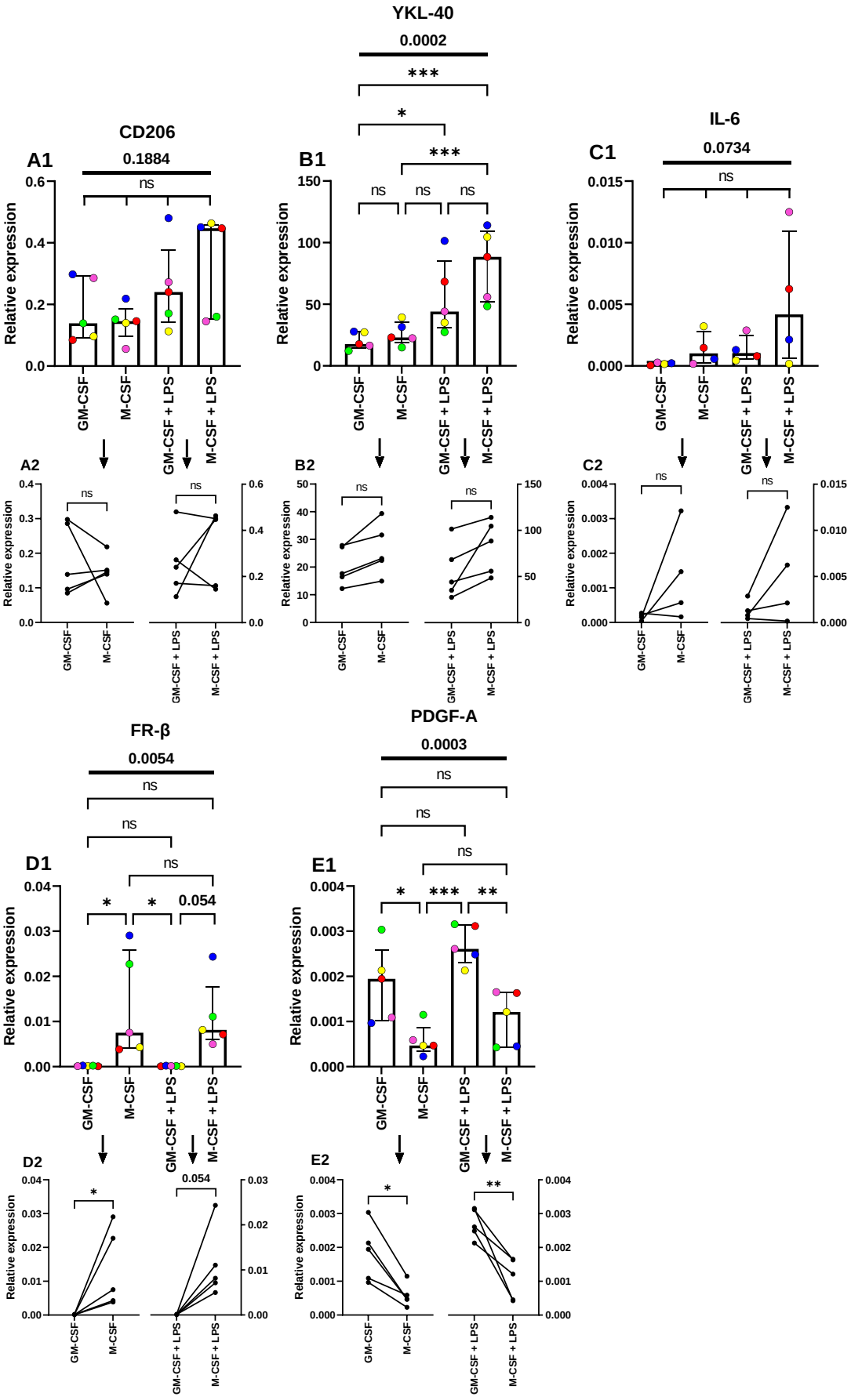

Figure 4. No distinct expression pattern of CD206, YKL-40, and IL-6 in unstimulated and stimulated GM/M-MØs and higher expression of FR-β in M-MØs and PDGF-A in GM-MØs.

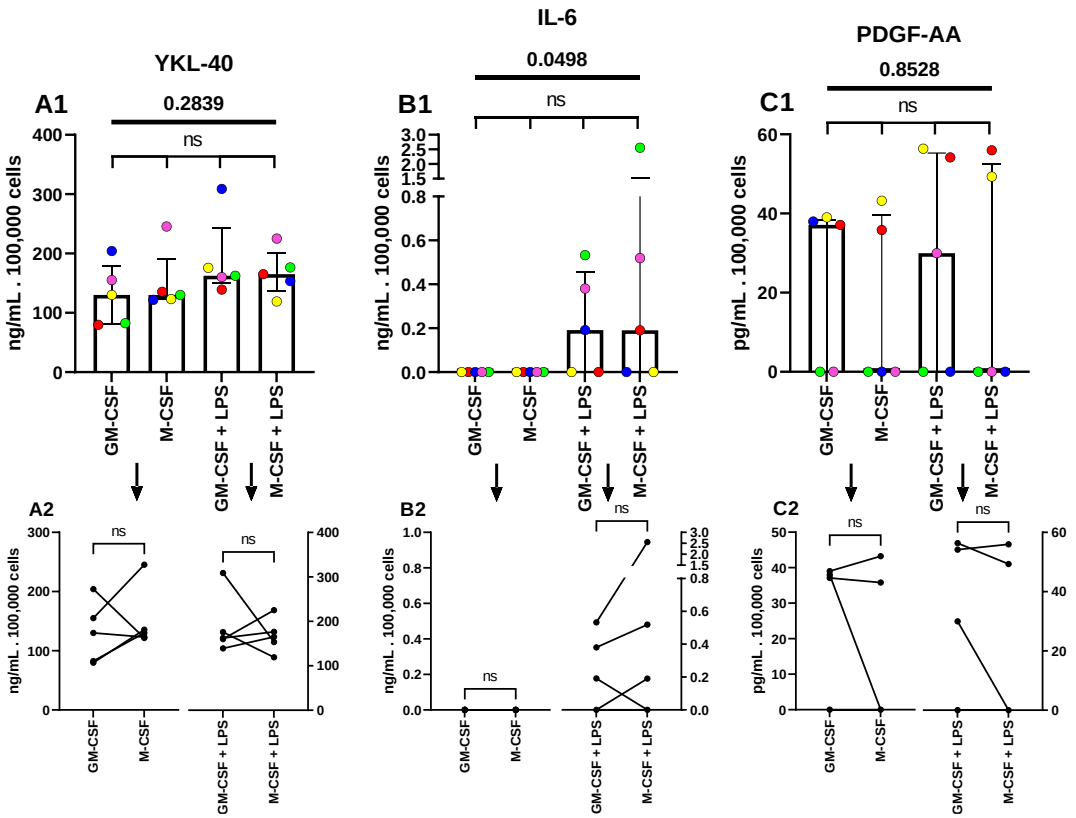

Figure 5. No distinct protein level pattern of YKL-40, IL-6, and PDGF-AA in unstimulated and stimulated GM/M-MØs.

3.2. No differential effect of GM/M-MØs on fibroblast migration and proliferation

The crosstalk between MØs and fibroblasts was studied using a fibroblast proliferation (MTT assay) and migration (scratch assay) assays in the presence of culture supernatant of unstimulated and stimulated GM/M-MØ. The following describes the MTT and scratch assay results with MØ culture supernatants of detached GM/M-MØs that were either unstimulated and stimulated at a normalized cell number.

Regarding fibroblast proliferation, no significant differences were seen between the different MØ conditions (Figure 6-A). In addition, there was no indication that stimulated MØs had more effect on fibroblast proliferation compared to unstimulated MØs. Overall, MØ culture supernatant was not a strong inducer of fibroblast proliferation. However, another explanation for this is that the sensitivity of the assay was lower than expected, due to the high cell density in the final MTT assay (Appendix 6.2). Besides, the GM/M-MØ phenotypes must also be considered, as is shown in Results 3.1 that these do not match the previously reported phenotypes. Altogether, the uncharacteristic MØ phenotypes and the lower sensitivity of the MTT assay make it hard to draw definitive conclusions on the effect of GM/M-MØ culture supernatants on fibroblast proliferation.

As for fibroblast migration, also no significant differences were seen between the different MØ conditions at both 16 and 24 hours post-scratch application (Figure 6-B/C). In addition, it was observed that fibroblast migration mainly occurred in the first 16 hours post-scratch application compared to the 8 hours thereafter. Even though no significant differences were seen between unstimulated and stimulated GM/M-MØs, it is interesting to note that MØs performed remarkably better compared to the negative control (low-serum growth medium only) with approximately two to three times more fibroblast migration for 16 and 24 hours post-scratch application (Figure 6-B/C). This demonstrates that the scratch assay has a high sensitivity between. However, due to the uncharacteristic MØ

phenotypes similar as with the results of the proliferation assay, it is hard to draw conclusions on the effect of GM/M-MØ culture supernatants on fibroblast migration.

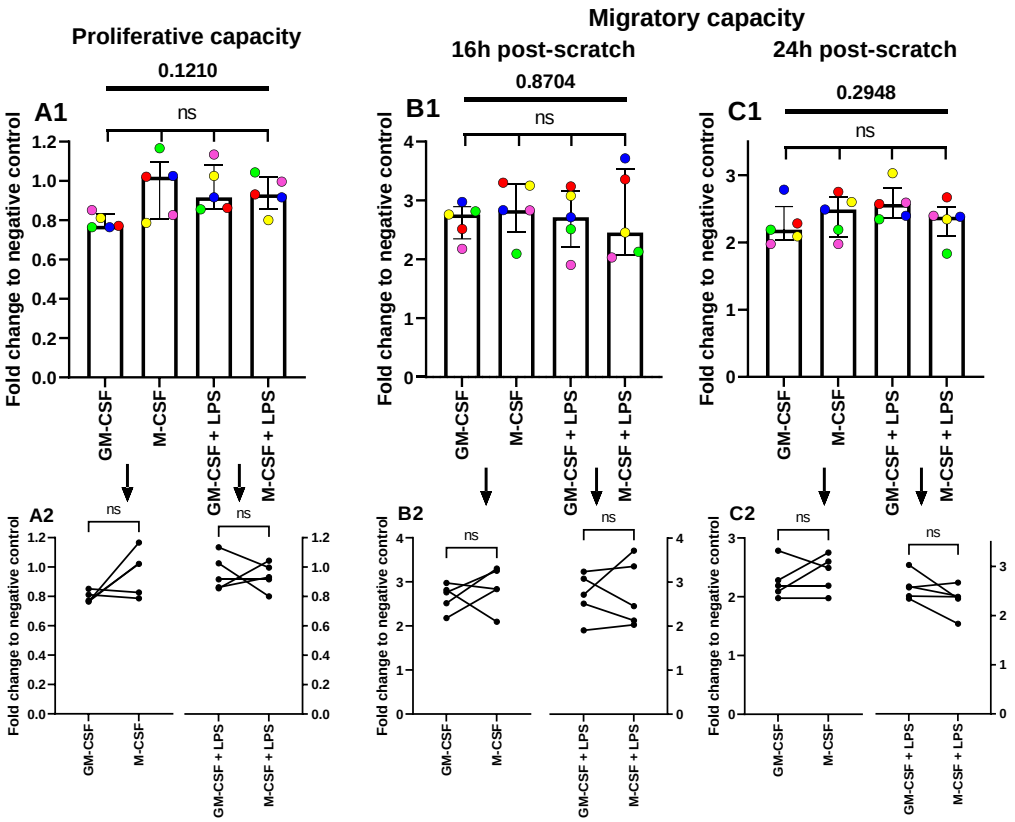

Figure 6. No differential effect of unstimulated and stimulated GM/M-MØ culture supernatants on fibroblast proliferation and migration.

3.3. Undetached MØs show no full restoration of characteristic GM/M-MØ expression pattern

It was suggested that the uncharacteristic GM/M-MØ phenotypes (Results 3.1) were caused by the detachment and re-seeding (at a normalized cell number) of MØs for activation. MØ detachment, re-seeding (cell attachment), and LPS activation may be too strong stressors for the skewed MØs and may have modulated the expression patterns of the markers studied. Therefore, GM/M-MØs were also activated without detachment followed by the addition of regular growth medium with or without GM/M-CSF for the last 24 hours. It was expected that adding GM/M-CSF for an additional 24 hours might further improve the expression pattern of GM/M-MØs towards the characteristic expression pattern of these MØs. The following describes the qPCR and ELISA results of undetached and stimulated GM/M-MØs with or without extra GM/M-CSF.

At the mRNA level, a tendency was seen for CD206 and IL-6 towards higher expression in M-MØs compared to GM-MØs (Figure 7-A/C). In contrast, IL-6 protein levels were higher in GM-MØs compared to M-MØs (Figure 8-B). Interestingly, for YKL-40, a tendency was observed with higher expression in GM-MØs compared to M-MØs (Figure 7-B). This tendency for YKL-40 was less pronounced at the protein level, although, this might also be due to donor variation (Figure 8-A). In general, no differences were seen between the expression pattern of MØs with or without the additional exposure to GM/M-CSF (Figure 7-A/B/C and Figure 8-A/B). When comparing the relative expression and protein levels of undetached with detached MØs (Results 3.1), a remarkable increase in expression of CD206, YKL-40, and IL-6 was observed. This was especially seen for YKL-40 and IL-6 with an approximate ten-fold increase at the mRNA and protein level, illustrating the effect of cell detachment on expression levels.

However, without the MØ detachment, the characteristic GM-MØ expression pattern is not fully restored, especially with respect to CD206 and IL-6 expression (mRNA level). Moreover, additional exposure to GM-CSF did not improve the expression pattern.

For FR-β expression, a distinct pattern was observed with high expression in M-MØs and minimal expression in GM-MØs (Figure 7-C). For PDGF-A(A), a tendency was found with high mRNA and protein levels in GM-MØs compared to M-MØs (Figure 7-E and Figure 8-C). Similarly, no differences were seen between the expression pattern of MØs with or without the additional exposure to GM/M-CSF (Figure 7-D/E and Figure 8-C). For FR-β, no increase in expression was seen for undetached compared to detached MØs (Results 3.1). For PDGF-A(A), this was also observed at mRNA level, however, at the protein level a strong increase was seen for undetached MØs compared to detached MØs. Altogether, no differences in FR-β and PDGF-A(A) expression were found between detached and undetached GM/M-MØs, further indicating that detachment of the MØs perse is not the cause of the uncharacteristic GM/M-MØs expression pattern.

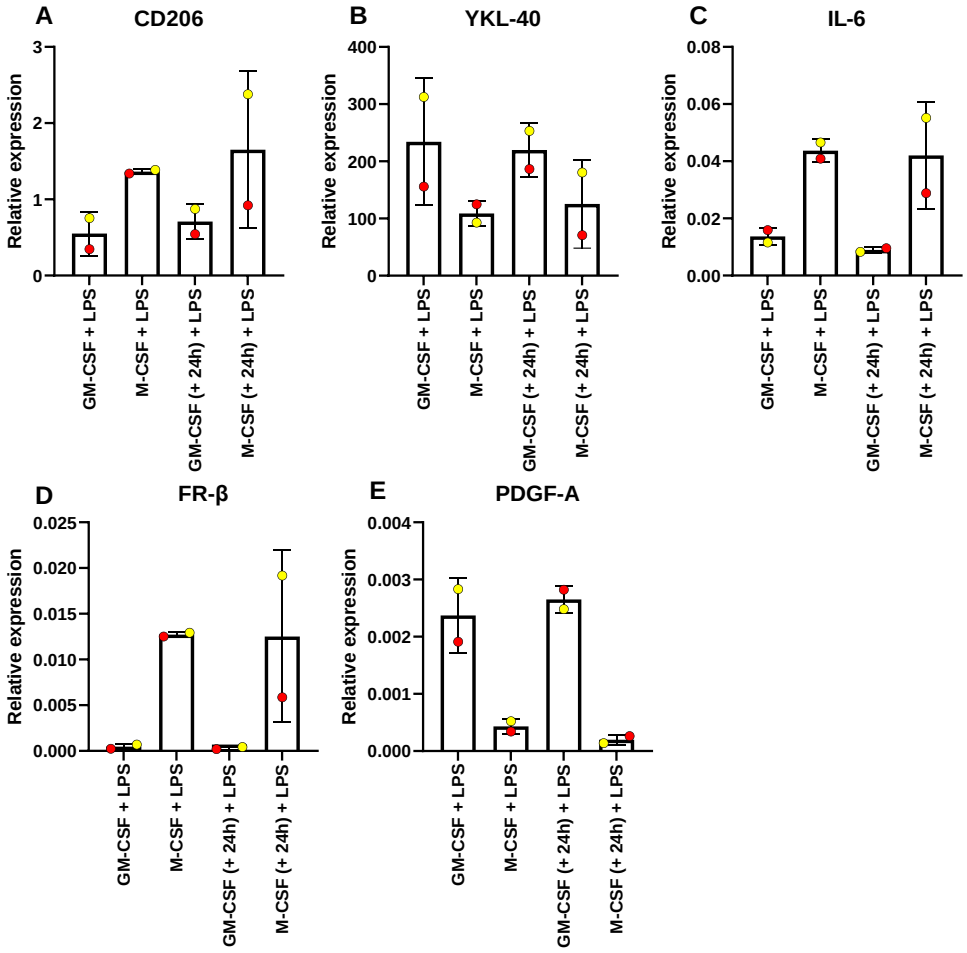

Figure 7. A tendency for high CD206, IL-6, and FR-β expression in M-MØs and high YKL-40 and PDGF-A expression in GM-MØs.

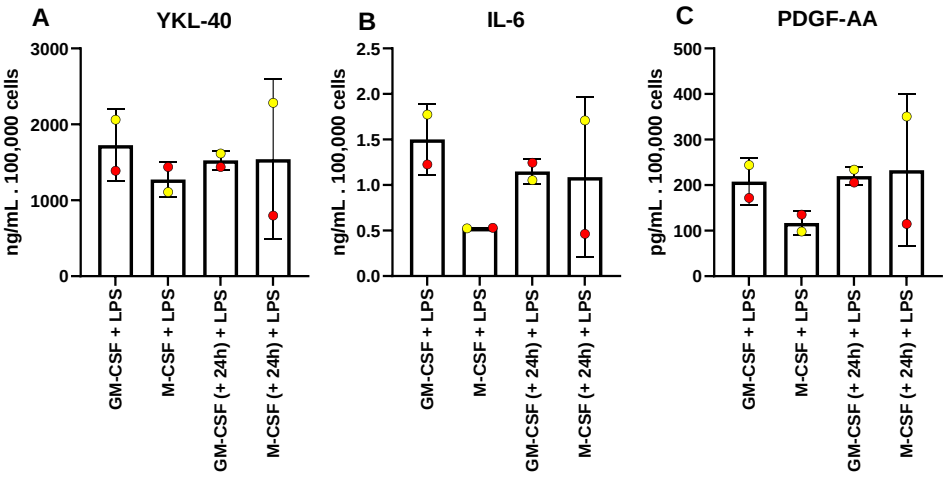

Figure 8. No strong tendency for YKL-40 protein levels in GM/M-MØs and a tendency for high IL-6 and PDGF-AA protein levels in GM-MØs.

4. DISCUSSION

4.1. Overview

This study focused on the interaction between GM/M-MØs and fibroblasts in GCA to further aid the development of new disease biomarkers, specific diagnostics, or targeted therapies for this disease. This crosstalk is crucial in the pathogenesis of GCA since it has been proposed that GM/M-MØs mediate fibroblast proliferation and migration from the adventitia to the intima, leading to intimal hyperplasia and ultimately vessel occlusion. It was hypothesized that the effectors of GM/M-MØs on fibroblasts are YKL-40 and PDGF-AA, respectively. Furthermore, it was expected that GM-MØs mainly mediate fibroblast migration, whereas M-MØs are important for both migration and proliferation of fibroblasts. To elucidate the extent of GM/M-MØs on fibroblast proliferation and migration, HC monocytes were differentiated in the presence of GM/M-CSF into GM/M-MØs. From here, MØ culture supernatants were used to study the effect of GM/M-MØ on *in vitro* fibroblast proliferation (MTT assay) and migration (scratch assay) using HC fibroblasts.

Before the assessment of fibroblast proliferation and migration, GM/M-MØs were analyzed for their characteristic expression pattern as previously reported and seen in GCA lesions [45,46,47]. However, no elevated CD206, YKL-40, and IL-6 expression was seen in GM-MØs compared to M-MØs, which are typical markers for GM-MØs within GCA lesions. On the other hand, the distinct pattern of high FR-β expression in M-MØs but not in GM-MØs was confirmed. For PDGF-A expression, the opposite pattern was observed with significant higher expression in GM-MØs compared to M-MØs, which is in contrast to what has been reported previously [45,52].

The uncharacteristic GM/M-MØ phenotypes might also the reason why no significant differences were observed between unstimulated and stimulated GM/M-MØs for fibroblast proliferation and migration. For the GM-MØ typical markers CD206, YKL40, and IL-6, it was seen that both GM-MØs and M-MØs display similar levels of these surface markers and executors. Meanwhile, it was seen that GM-MØs and M-MØs display both M-MØ typical markers. GM-MØs showed elevated PDGF-A expression, whereas M-MØs showed FR-β expression. Collectively, the overlap in YKL-40 expression and the contrasting expression of PDGF-AA made it hard to assess the direct effect of GM-MØs or M-MØs on fibroblast proliferation and migration with regard to the proposed role of GM/M-MØs in GCA.

4.2. Possible explanations for uncharacteristic GM/M-MØ expression pattern

The uncharacteristic GM/M-MØ phenotypes seen in our experiments were not in line with previous reports that studied MØ skewing by GM/M-CSF [40,45,46,47]. Hence, possible explanations were sought to explain the uncharacteristic GM/M-MØ expression patterns observed for CD206, YKL-40, IL-6, and PDGF-A.

Detachment and re-seeding

The first factors we explored were the detachment and re-seeding of the skewed GM/M-MØs necessary for MØ activation at a normalized cell number. To study the interaction between GM/M-MØs and fibroblasts, an *in vitro* protocol was envisioned where MØ culture supernatant was used to assess proliferative and migratory capacities of fibroblasts. Because of this setup, MØ culture supernatant had to be harvested from a MØ culture with a normalized cell number, so that fibroblast behavior could only be influenced by the difference in MØ production of soluble mediators and not by the number of MØs. Regarding the MØ detachment, it was found by others that this downregulated M2-MØ markers CD163 and CD206 in polarized MØs when detachment was done using enzymatic

reagents like trypsin [53,54]. Furthermore, the stress of MØ detachment in conjunction with re-seeding may also further disturb the initial phenotype displayed by the polarized MØs [55,56].

To address whether detachment and re-seeding are responsible for the uncharacteristic phenotypes seen in detached GM/M-MØs, other MØs were cultured and activated under similar conditions but without detachment. Altogether, these experiments showed that undetached MØs do not fully restore the characteristic GM/M-MØ expression pattern since only insignificant shifts were seen towards more YKL-40 and IL-6 expression in GM-MØs. Of note, no detachment of MØs strongly increased CD206 expression and PDGF-AA protein levels and massively enhanced YKL-40 and IL-6 mRNA and protein levels compared to detached MØs, indicating that detachment does affect the level of expression to a certain extent.

LPS stimulation and stimulation length

Since MØ detachment and re-seeding was probably not at cause of the uncharacteristic GM/M-MØ phenotypes, it was suggested that other factors regarding the protocol or culture conditions might have play a role. In particular, the use of LPS for MØ stimulation needs to be evaluated. It was already established that MØs may display a mix of both M1- and M2-MØ traits [43]. However, because of the incredible plasticity of MØs, this phenotype can also rapidly change depending on signals from the microenvironment [37,38]. Thus, it may be suggested that stimulation of LPS on polarized MØs results in an alteration of expression patterns and not in the expected increase of expression of the markers that were already expressed. In line with this is that stimulation with LPS alone or in combination with IFN-γ is often used for generating MØs showing M1-MØ traits [37,40,57,58].

Regarding the detached GM/M-MØs in our experiments, it may be that LPS stimulation diminished CD206 expression in both MØ subsets since CD206 is a marker for M2-MØs. Indeed, increased CD206 expression in GM-MØs compared to M-MØs was found in another study using unstimulated HC MØs [45]. Nonetheless, if this was the case, than still a higher CD206 expression would be expected for the unstimulated (detached) GM-MØs compared to M-MØs. Moreover, for undetached MØs, which were all stimulated with LPS, a tendency was still observed towards higher CD206 expression in M-MØs. For FR-β expression, also a marker for M2-MØs [59], also no downregulation was seen for stimulated compared to unstimulated MØs. Overall, this indicated that LPS stimulation was not a major contributor to the uncharacteristic GM/M-MØ expression pattern of CD206. However, LPS might have affected the IL-6 expression of both detached and undetached GM/M-MØs. It is well known that LPS causes the upregulation of pro-inflammatory cytokines like IL-6 in MØs [60], which could explain that IL-6 expression is only seen in stimulated MØs albeit at similar levels in GM- and M-MØs.

LPS stimulation length may also influence CD206 expression. One study showed that M2-MØ markers like CD206 need two to three days of stimulation with IL-4 to reach the highest expression on polarized MØs [61], whereas in our study we only used four hours stimulation with LPS. This could give an indication on the kinetics of CD206 expression in polarized MØs. Besides, in a study by Van Sleen et al. (2021) two days of LPS stimulation on polarized GM/M-MØs had resulted in similar YKL-40 expression levels with no distinct YKL-40 expression pattern for HC MØs [47]. This indicates that LPS stimulation length alone cannot explain the YKL-40 expression pattern observed in our experiments. Finally, higher PDGF-A expression levels in M-MØs compared to GM-MØs have been reported upon two days LPS stimulation on polarized MØs [45]. In our current study, the opposite expression pattern was seen after four hours of stimulation on polarized MØs, perhaps indicating that PDGF-A expression is influenced by the length of stimulation.

Monocyte isolation, GM/M-CSF concentration, and presence of GM/M-CSF

Other factors that might have influenced the GM/M-MØ expression pattern are the monocyte isolation method, GM/M-CSF concentration, and presence of GM/M-CSF. For this study, monocytes were isolated from HC PBMCs using separation based on Percoll® gradients followed by culture adherence. The distinct GM/M-MØ expression pattern was seen in MØs cultured from HC monocytes that were isolated by negative selection using the EasySep monocyte enrichment kit, which does not deplete $CD16^+$ monocytes [45,47]. However, this difference in monocyte isolation method should not have had such a significant impact. It was established by flow cytometry that only after separation by Percoll® gradients, a monocyte purity of 67% was reached whilst containing all monocyte subsets (Appendix 6.1). The additional four hours culture adherence followed by washing further depleted non-adherent lymphocytes [62] from the monocyte culture. Although, lymphocytes can react to GM-CSF [63], subsequent washing during the medium change at days three and five should have removed remaining lymphocytes and further increased the purity of the monocyte-derived MØs.

In our study monocytes were differentiated into GM/M-MØs in the presence of 50 ng/mL GM/M-CSF, whereas in the study of Jiemy et al. (2020) and Van Sleen et al. (2021) 100 ng/mL GM/M-CSF was used [45,47]. At first, this difference in concentration seems significant enough to explain the uncharacteristic GM/M-MØ expression pattern. However, in other studies similar or even lower concentrations of GM-CSF or M-CSF have been used, where still significant phenotypic differences were induced between the polarized MØ subsets [61,64,65,66].

In the studies by Jiemy et al. (2020) and Van Sleen et al. (2021) MØs were differentiated into GM/M-MØs with their characteristic expression pattern according to a protocol where GM/M-CSF was continuously present in the culture medium [45,47]. For MØ differentiation in this study, GM/M-CSF was not added in the culture medium after MØ activation of detached MØs, because MØ culture supernatants was later on used for the fibroblast proliferation and migration assay. This MØ culture supernatant should not contain GM/M-CSF, because these factors could have also influenced the fibroblasts directly. For example, it has been shown that GM-CSF causes proliferation in a dermal fibroblast cell line [67]. Thus, ideally the obtained MØ culture supernatant should only contain the soluble factors produced by the GM/M-MØs. To investigate the effect of the removal of GM/M-CSF, undetached GM/M-MØs were cultured with or without GM/M-CSF for the last 24 hours after MØ activation. However, similar CD206, YKL-40, IL-6, FR-β, and PDGF-A(A) expression was seen between MØs with the additional GM/M-CSF exposure and those without. Altogether, we believe it is unlikely that differences in monocyte isolation method, GM/M-CSF concentration, and GM/M-CSF presence are the cause of the uncharacteristic GM/M-MØ expression pattern.

Low-glucose DMEM

As a final potential modulating factor of the MØ expression pattern, we evaluated the effects of low-glucose DMEM used for culturing of MØs in this study. The decision to culture MØs with DMEM was because at the end the MØ culture supernatant was used in the fibroblast proliferation and migration assay. Earlier, our group established that primary human dermal fibroblasts grow best in DMEM and not well in the standard used RPMI. Thus, to rule out the effect of RPMI on fibroblasts, MØs were cultured in DMEM instead of RPMI. Moreover, low-glucose DMEM (1 g/L glucose) instead of high-glucose DMEM (4.5 g/L glucose) was used to minimize the effect of glucose on fibroblast proliferation and migration since it has been reported that very high levels of glucose can impair fibroblast proliferation and migration [68].

It is now well established that certain metabolic activities are directly linked to the phenotype of immune cells [41]. Major metabolic pathways present in cells comprise glycolysis, pentose phosphate

pathway (PPP), oxidative phosphorylation (OXPHOS), and fatty acid oxidation (FAO) [69]. Whereas the quickly initiated glycolysis and the PPP mainly fuel on glucose, a combination of OXPHOS and FAO sustains long-term metabolism that is less dependent on glucose [70]. Overall, metabolic pathways are linked via the TCA cycle [69]. MØs activated by M1-MØ stimuli like LPS or IFN-γ mainly rely on glycolysis and the PPP for their rapid production of pro-inflammatory mediators, whereby OXPHOS is downregulated [41,69]. In these activated MØs, there is also a break in the TCA cycle that results in the accumulation of citrate and succinate, which respectively contribute to tissue-destructive mediators such as NO and ROS and pro-inflammatory cytokines like IL-1β and IL-6 [41,70]. Interestingly, two main molecular pathways responsible for the switch to this pro-inflammatory and tissue-destructive metabolic phenotype are activated by GM-CSF and LPS [71]. In contrast, MØs activated by M2-stimuli show upregulation of FAO and OXPHOS and are therefore more energetically stable on the long-term, which is believed to be necessary for the prolonged responses in these MØs [41,69]. These MØs have an intact TCA cycle, which allows them to use the electron transport chain for the generation of energy [71]. Interestingly, it has been discovered that next to the use of OXPHOS, these MØs also may use glycolysis [72], where it was seen that both are upregulated by M-CSF [73]. This deployment of both OXPHOS and glycolysis makes these MØs very flexible when energy substrates like glucose are scarce [72].

Thus, it can be postulated that pro-inflammatory and tissue-destructive MØs skewed by LPS and GM-CSF display the inflexible glycolysis and PPP metabolic pathways, whereas tissue-remodeling MØs skewed by M-CSF are more flexible using OXPHOS, FAO, and if needed glycolysis. It is expected that the use of low-glucose DMEM is reflected in the GM/M-MØ expression pattern due to the characteristic metabolic phenotypes seen in these MØs. It is suggested that the MØs polarized by GM-CSF solely use glycolysis and PPP to support their differentiation into $CD206^+$ MØs. However, because of the scarcity of glucose, they are unable to overexpress their markers. The additional stimulation with LPS may further increased the need for glucose and hence impair marker expression. On the other hand, MØs polarized by M-CSF show more flexibility by displaying OXPHOS, FAO, and glycolysis, thereby having less difficulty with low-glucose conditions, leading to a basal level of expression of their surface markers. This may explain why CD206 is expressed at a similar level between GM/M-MØs. In line with this is the overexpression of FR-β in M-MØs compared to GM-MØs, which still confirmed the typical FR-β expression seen in M-MØs. Along this line, also IL-6 expression between GM/M-MØs can be explained where a scarcity in glucose makes GM-MØs unable to overexpress IL-6 compared to M-MØs [74]. Similarly, the same reasoning may explain YKL-40 expression by GM/M-MØs, although, other previously mentioned explanations may also apply here.

Indeed, other *in vitro* studies showing differences in expression pattern of GM/M-MØs have been performed using RPMI (4.5 g/L glucose) and not low-glucose DMEM [45,47,61,64,65,66,75]. Moreover, earlier in this project and in another project (Appendix 6.5), MØs were skewed and activated into GM/M-MØs using RPMI as culture medium. In here, it was shown that the expression pattern of CD206, YKL-40, IL-6, FR-β, and PDGF-A was perfectly in line with previous studies from Jiemy et al. (2020) and Van Sleen et al. (2021) [45,47]. Collectively, indicating the significance of the glucose concentration in culture medium during GM/M-MØ polarization. Altogether, these observations stress the importance of glucose concentrations in culture medium and culture medium composition in general, when designing *in vitro* experiments exploring cell behavior.

4.3. Future perspectives

Collectively, all aforementioned factors need to be taken into account for the explanation of the expression pattern of GM/M-MØs in this study, although, individual factors likely contributed to

different degrees. The variety of influencing factors were at the end all necessary for the main goal of this study, that is exploring the crosstalk between GM/M-MØs and fibroblasts. Whereas other studies solely focused on the expression pattern of polarized MØs, this study tried to mimic the interaction between MØs and their environment in an *in vitro* model. Unfortunately, these decisions lead to the uncharacteristic GM/M-MØ expression pattern, resulting in no further insight in the relation between GM/M-MØs and fibroblasts. However, still important lessons can be learned from this study to aid future research.

Besides the main focus on the crosstalk of MØs and fibroblasts in GCA, we also optimized the condition for the MTT (proliferation) and scratch (migration) assay. In general, the MTT and scratch assay are simple, straightforward, and cheap methods to quantify the proliferative and migratory capacities of fibroblasts, yet these assays did require optimization. One flaw of these assays was that they required a constant cell seeding density for a proper outcome. This cell seeding density was especially important for the MTT assay since it ensured the maximum sensitivity window for that assay. Unfortunately, due to practical limitations with cell counting, it was difficult to ensure a constant seeding density, even when the optimal seeding density was known. Altogether, this represents another limitation of this study. Additionally, also no optimal positive control for both assays was found. All these limitations and optimizations are discussed more elaborately in Appendix 6.2 and 6.3.

Regarding these limitations, future studies assessing fibroblast behavior in the presence of MØ culture supernatants could tend towards alternative assays that have more reliable outcomes. Instead of using MTT in the proliferation assay, also XTT (2,3-bis-(2-methoxy-4-nitro-5-sulfophenyl), MTS (methyl trichlorosilane), or WST1 (water soluble tetrazolium 1) can be utilized, which also reflect metabolic activity [76]. The advantage over MTT is that for these compounds the formed crystals directly dissolve in the medium, which allows continuous monitoring of fibroblast proliferation. Cell proliferation or viability markers can also be targeted such as Ki-67 using antibodies [77] or ATP using luciferase [76], respectively. These methods allow more accurate and sensitive assessment of fibroblast proliferation. Improvements for the scratch assay mainly consist of tools that aid scratch application or increase the reproducibility of the scratch application. Tools that aid scratch application usually serve as a guide for the micropipette tip such as a slit on top of the well. The reproducibility of the scratch can be increased using tools that allow for constant cell removal such as a strip or stopper that is applied before cell seeding [78]. Next to the conventional scratch assay, an on-chip or Transwell migration assay may also be utilized. The on-chip migration assay allows for automated and precise wounding with a good reproducibility [79], whereas the Transwell enables precise quantification of migration by staining cells that have migrated through a permeable membrane [80]. Both tools ensure proper assessment of fibroblast migration with a constant outcome. Besides, also other state of the art tools may be utilized to study cell interactions in GCA, such as the use of *ex vivo* cultured arteries of GCA patients [81].

In case the improvements of the fibroblast proliferation and migration assay are accomplished, still the interaction between GM/M-MØs and fibroblasts needs to be implemented. Earlier, a variety of factors that influence the GM/M-MØ expression pattern was discussed. It was proposed that the use of low-glucose DMEM mainly affected the expression pattern of MØs, whereas other potentially cofounding factors are deemed less important. Thus, for future studies assessing fibroblast proliferation and migration in the presence of GM/M-MØ culture supernatant, it is important to culture MØs in a culture medium that contains sufficient glucose (around 4.5 g/L), such as high-glucose DMEM or regular RPMI. Though, a mimic of the *in vivo* situation would be most preferable. The normalization of the number of MØs by detachment and re-seeding can still be done since it was shown that detached and undetached MØs show similar expression patterns. Furthermore, it was shown that detached GM/M-MØs cultured in RPMI (4.5 g/L glucose) displayed the characteristic

GM/M-MØ expression pattern (Appendix 6.5). If in future studies the interaction between MØs and fibroblasts is assessed in a similar setup as reported here, it is advised to culture MØs as well as fibroblasts in high-glucose DMEM. In this way, the effect of the characteristic GM/M-MØs on fibroblast behavior can still be studied by using MØ culture supernatant in the fibroblast proliferation and migration assays. Although, there might be a (minimal) inhibitory effect of high-glucose on fibroblast proliferation and migration, such an effect would be similar for all test conditions. For future studies, these changes would still allow investigating the crosstalk between GM/M-MØs and fibroblasts with the same setup as described in this study, thereby hopefully contributing to the knowledge of GCA pathogenesis.

5. CONCLUSION

Altogether, this study did not establish a difference in fibroblast proliferation and migration between GM/M-MØs due to uncharacteristic GM/M-MØ expression pattern likely caused by the use of low-glucose DMEM. For future studies, it is advised to culture MØs in high-glucose DMEM and to use sensitive fibroblast proliferation and migration assays to assess the crosstalk between GM/M-MØs and fibroblasts. Overall, showing that careful consideration of culture conditions is crucial for *in vitro* approaches of MØ polarization and their effect on fibroblast proliferation and migration.

6. REFERENCES

1. Samson, M., Corbera-Bellalta, M., Audia, S., Planas-Rigol, E., Martin, L., Cid, M. C., & Bonnotte, B. (2017). Recent advances in our understanding of giant cell arteritis pathogenesis. *Autoimmunity Reviews*, *16*(8), 833–844. https://doi.org/10.1016/j.autrev.2017.05.014
2. Hunder, G. G., Bloch, D. A., Michel, B. A., Stevens, M. B., Arend, W. P., Calabrese, L. H., Edworthy, S. M., Fauci, A. S., Leavitt, R. Y., Lie, J. T., Lightfoot, R. W., Masi, A. T., McShane, D. J., Mills, J. A., Wallace, S. L., & Zvaifler, N. J. (2010). The American College of Rheumatology 1990 criteria for the classification of giant cell arteritis. *Arthritis & Rheumatism*, *33*(8), 1122–1128. https://doi.org/10.1002/art.1780330810
3. Jennette, J. C., Falk, R. J., Bacon, P. A., Basu, N., Cid, M. C., Ferrario, F., Flores-Suarez, L. F., Gross, W. L., Guillevin, L., Hagen, E. C., Hoffman, G. S., Jayne, D. R., Kallenberg, C. G. M., Lamprecht, P., Langford, C. A., Luqmani, R. A., Mahr, A. D., Matteson, E. L., Merkel, P. A., … Watts, R. A. (2013). Revised International Chapel Hill Consensus Conference Nomenclature of Vasculitides. *Arthritis & Rheumatism*, *65*(1), 1–11. https://doi.org/10.1002/art.37715
4. Koster, M. J., Matteson, E. L., & Warrington, K. J. (2018). Large-vessel giant cell arteritis: diagnosis, monitoring and management. *Rheumatology*, *57*(suppl_2), ii32–ii42. https://doi.org/10.1093/rheumatology/kex424
5. Fernandes Serôdio, J., Trindade, M., Favas, C., & Delgado Alves, J. (2021). Extra-Cranial Involvement in Giant Cell Arteritis. In *Giant-Cell Arteritis [Working Title]*. IntechOpen. https://doi.org/10.5772/intechopen.97715
6. Borchers, A. T., & Gershwin, M. E. (2012). Giant cell arteritis: A review of classification, pathophysiology, geoepidemiology and treatment. *Autoimmunity Reviews*, *11*(6–7), A544–A554. https://doi.org/10.1016/j.autrev.2012.01.003
7. Seetharaman, M. (2020). Giant Cell Arteritis (Temporal Arteritis). *Medscape*.
8. Li, K. J., Semenov, D., Turk, M., & Pope, J. (2021). A meta-analysis of the epidemiology of giant cell arteritis across time and space. *Arthritis Research & Therapy*, *23*(1), 82. https://doi.org/10.1186/s13075-021-02450-w
9. Salvarani, C., Cantini, F., & Hunder, G. G. (2008). Polymyalgia rheumatica and giant-cell arteritis. *The Lancet*, *372*(9634), 234–245. https://doi.org/10.1016/S0140-6736(08)61077-6
10. Sharma, A., Mohammad, A. J., & Turesson, C. (2020). Incidence and prevalence of giant cell arteritis and polymyalgia rheumatica: A systematic literature review. *Seminars in Arthritis and Rheumatism*, *50*(5), 1040–1048. https://doi.org/10.1016/j.semarthrit.2020.07.005
11. Dejaco, C., Duftner, C., Buttgereit, F., Matteson, E. L., & Dasgupta, B. (2016). The spectrum of giant cell arteritis and polymyalgia rheumatica: revisiting the concept of the disease. *Rheumatology*, kew273. https://doi.org/10.1093/rheumatology/kew273
12. Nuenninghoff, D. M., Hunder, G. G., Christianson, T. J. H., McClelland, R. L., & Matteson, E. L. (2003). Incidence and predictors of large-artery complication (aortic aneurysm, aortic dissection, and/or large-artery stenosis) in patients with giant cell arteritis: A population-based study over 50 years. *Arthritis & Rheumatism*, *48*(12), 3522–3531. https://doi.org/10.1002/art.11353
13. Salvarani, C., Pipitone, N., Versari, A., & Hunder, G. G. (2012). Clinical features of polymyalgia rheumatica and giant cell arteritis. *Nature Reviews Rheumatology*, *8*(9), 509–521. https://doi.org/10.1038/nrrheum.2012.97
14. Alba, M. A., García-Martínez, A., Prieto-González, S., Tavera-Bahillo, I., Corbera-Bellalta, M., Planas-Rigol, E., Espígol-Frigolé, G., Butjosa, M., Hernández-Rodríguez, J., & Cid, M. C. (2014).

Relapses in Patients With Giant Cell Arteritis. *Medicine*, *93*(5), 194–201. https://doi.org/10.1097/MD.0000000000000033
15. Ponte, C., Martins-Martinho, J., & Luqmani, R. A. (2020). Diagnosis of giant cell arteritis. *Rheumatology*, *59*(Supplement_3), iii5–iii16. https://doi.org/10.1093/rheumatology/kez553
16. Sebastian, A., Coath, F., Innes, S., Jackson, J., van der Geest, K. S. M., & Dasgupta, B. (2021). Role of the halo sign in the assessment of giant cell arteritis: a systematic review and meta-analysis. *Rheumatology Advances in Practice*, *5*(3). https://doi.org/10.1093/rap/rkab059
17. Klein, R. G., Campbell, R. J., Hunder, G. G., & Carney, J. A. (1976). Skip lesions in temporal arteritis. *Mayo Clinic Proceedings*, *51*(8), 504–510.
18. Brack, A., Martinez-Taboada, V., Stanson, A., Goronzy, J. J., & Weyand, C. M. (1999). Disease pattern in cranial and large-vessel giant cell arteritis. *Arthritis & Rheumatism*, *42*(2), 311–317. https://doi.org/10.1002/1529-0131(199902)42:2<311::AID-ANR14>3.0.CO;2-F
19. Jiemy, W. F., Heeringa, P., Kamps, J. A. A. M., van der Laken, C. J., Slart, R. H. J. A., & Brouwer, E. (2018). Positron emission tomography (PET) and single photon emission computed tomography (SPECT) imaging of macrophages in large vessel vasculitis: Current status and future prospects. *Autoimmunity Reviews*, *17*(7), 715–726. https://doi.org/10.1016/j.autrev.2018.02.006
20. Chew, S. S. L., Kerr, N. M., & Danesh-Meyer, H. V. (2009). Giant cell arteritis. *Journal of Clinical Neuroscience*, *16*(10), 1263–1268. https://doi.org/10.1016/j.jocn.2009.05.002
21. Proven, A., Gabriel, S. E., Orces, C., O'Fallon, W. M., & Hunder, G. G. (2003). Glucocorticoid therapy in giant cell arteritis: Duration and adverse outcomes. *Arthritis & Rheumatism*, *49*(5), 703–708. https://doi.org/10.1002/art.11388
22. Cid, M. C., Ríos-Garcés, R., Terrades-García, N., & Espígol-Frigolé, G. (2020). Treatment of giant-cell arteritis: from broad spectrum immunosuppressive agents to targeted therapies. *Rheumatology*, *59*(Supplement_3), iii17–iii27. https://doi.org/10.1093/rheumatology/kez645
23. Ma-Krupa, W., Jeon, M.-S., Spoerl, S., Tedder, T. F., Goronzy, J. J., & Weyand, C. M. (2004). Activation of Arterial Wall Dendritic Cells and Breakdown of Self-tolerance in Giant Cell Arteritis. *Journal of Experimental Medicine*, *199*(2), 173–183. https://doi.org/10.1084/jem.20030850
24. Ma-Krupa, W., Kwan, M., Goronzy, J., & Weyand, C. (2005). Toll-like receptors in giant cell arteritis. *Clinical Immunology*, *115*(1), 38–46. https://doi.org/10.1016/j.clim.2005.02.009
25. Krupa, W. M., Dewan, M., Jeon, M.-S., Kurtin, P. J., Younge, B. R., Goronzy, J. J., & Weyand, C. M. (2002). Trapping of Misdirected Dendritic Cells in the Granulomatous Lesions of Giant Cell Arteritis. *The American Journal of Pathology*, *161*(5), 1815–1823. https://doi.org/10.1016/S0002-9440(10)64458-6
26. Weyand, C. M., & Goronzy, J. J. (2003). Medium- and Large-Vessel Vasculitis. *New England Journal of Medicine*, *349*(2), 160–169. https://doi.org/10.1056/NEJMra022694
27. Samson, M., Audia, S., Fraszczak, J., Trad, M., Ornetti, P., Lakomy, D., Ciudad, M., Leguy, V., Berthier, S., Vinit, J., Manckoundia, P., Maillefert, J.-F., Besancenot, J.-F., Aho-Glele, S., Olsson, N. O., Lorcerie, B., Guillevin, L., Mouthon, L., Saas, P., … Bonnotte, B. (2012). Th1 and Th17 lymphocytes expressing CD161 are implicated in giant cell arteritis and polymyalgia rheumatica pathogenesis. *Arthritis & Rheumatism*, *64*(11), 3788–3798. https://doi.org/10.1002/art.34647
28. Samson, M., Lakomy, D., Audia, S., & Bonnotte, B. (2011). T(H)17 lymphocytes: induction, phenotype, functions, and implications in human disease and therapy. *La Revue de Médecine Interne*, *32*(5), 292–301. https://doi.org/10.1016/j.revmed.2009.12.020
29. Corbera-Bellalta, M., Planas-Rigol, E., Lozano, E., Terrades-García, N., Alba, M. A., Prieto-González, S., García-Martínez, A., Albero, R., Enjuanes, A., Espígol-Frigolé, G., Hernández-

Rodríguez, J., Roux-Lombard, P., Ferlin, W. G., Dayer, J.-M., Kosco-Vilbois, M. H., & Cid, M. C. (2016). Blocking interferon γ reduces expression of chemokines CXCL9, CXCL10 and CXCL11 and decreases macrophage infiltration in ex vivo cultured arteries from patients with giant cell arteritis. *Annals of the Rheumatic Diseases*, *75*(6), 1177–1186. https://doi.org/10.1136/annrheumdis-2015-208371

30. Van Sleen, Y., Wang, Q., van der Geest, K. S. M., Westra, J., Abdulahad, W. H., Heeringa, P., Boots, A. M. H., & Brouwer, E. (2017). Involvement of Monocyte Subsets in the Immunopathology of Giant Cell Arteritis. *Scientific Reports*, *7*(1), 6553. https://doi.org/10.1038/s41598-017-06826-4
31. Samson, M., Ly, K. H., Tournier, B., Janikashvili, N., Trad, M., Ciudad, M., Gautheron, A., Devilliers, H., Quipourt, V., Maurier, F., Meaux-Ruault, N., Magy-Bertrand, N., Manckoundia, P., Ornetti, P., Maillefert, J.-F., Besancenot, J. F., Ferrand, C., Mesturoux, L., Labrousse, F., … Bonnotte, B. (2016). Involvement and prognosis value of CD8 + T cells in giant cell arteritis. *Journal of Autoimmunity*, *72*, 73–83. https://doi.org/10.1016/j.jaut.2016.05.008
32. Hernandez-Rodriguez, J. (2003). Tissue production of pro-inflammatory cytokines (IL-1 , TNF and IL-6) correlates with the intensity of the systemic inflammatory response and with corticosteroid requirements in giant-cell arteritis. *Rheumatology*, *43*(3), 294–301. https://doi.org/10.1093/rheumatology/keh058
33. Ly, K.-H., Régent, A., Tamby, M. C., & Mouthon, L. (2010). Pathogenesis of giant cell arteritis: More than just an inflammatory condition? *Autoimmunity Reviews*, *9*(10), 635–645. https://doi.org/10.1016/j.autrev.2010.05.002
34. Nikkari, S. T., Höyhtyä, M., Isola, J., & Nikkari, T. (1996). Macrophages contain 92-kd gelatinase (MMP-9) at the site of degenerated internal elastic lamina in temporal arteritis. *The American Journal of Pathology*, *149*(5), 1427–1433.
35. Kaiser, M., Younge, B., Björnsson, J., Goronzy, J. J., & Weyand, C. M. (1999). Formation of New Vasa Vasorum in Vasculitis. *The American Journal of Pathology*, *155*(3), 765–774. https://doi.org/10.1016/S0002-9440(10)65175-9
36. Kaiser, M., Weyand, C. M., Björnsson, J., & Goronzy, J. J. (1998). Platelet-derived growth factor, intimal hyperplasia, and ischemic complications in giant cell arteritis. *Arthritis & Rheumatism*, *41*(4), 623–633. https://doi.org/10.1002/1529-0131(199804)41:4<623::AID-ART9>3.0.CO;2-6
37. Shapouri-Moghaddam, A., Mohammadian, S., Vazini, H., Taghadosi, M., Esmaeili, S., Mardani, F., Seifi, B., Mohammadi, A., Afshari, J. T., & Sahebkar, A. (2018). Macrophage plasticity, polarization, and function in health and disease. *Journal of Cellular Physiology*, *233*(9), 6425–6440. https://doi.org/10.1002/jcp.26429
38. Zhang, H., Watanabe, R., Berry, G. J., Vaglio, A., Liao, Y. J., Warrington, K. J., Goronzy, J. J., & Weyand, C. M. (2017). Immunoinhibitory checkpoint deficiency in medium and large vessel vasculitis. *Proceedings of the National Academy of Sciences*, *114*(6), E970–E979. https://doi.org/10.1073/pnas.1616848114
39. Chávez-Galán, L., Olleros, M. L., Vesin, D., & Garcia, I. (2015). Much More than M1 and M2 Macrophages, There are also CD169+ and TCR+ Macrophages. *Frontiers in Immunology*, *6*. https://doi.org/10.3389/fimmu.2015.00263
40. Donne Estipona. (2020). A Guide to Macrophage Markers.
41. Esen, I., Jiemy, W. F., van Sleen, Y., van der Geest, K. S. M., Sandovici, M., Heeringa, P., Boots, A. M. H., & Brouwer, E. (2021). Functionally Heterogenous Macrophage Subsets in the Pathogenesis of Giant Cell Arteritis: Novel Targets for Disease Monitoring and Treatment. *Journal of Clinical Medicine*, *10*(21), 4958. https://doi.org/10.3390/jcm10214958

42. Martinez, F. O., Helming, L., & Gordon, S. (2009). Alternative Activation of Macrophages: An Immunologic Functional Perspective. *Annual Review of Immunology*, *27*(1), 451–483.
43. Sica, A., & Mantovani, A. (2012). Macrophage plasticity and polarization: in vivo veritas. *Journal of Clinical Investigation*, *122*(3), 787–795. https://doi.org/10.1172/JCI59643
44. Watanabe, S., Alexander, M., Misharin, A. v., & Budinger, G. R. S. (2019). The role of macrophages in the resolution of inflammation. *Journal of Clinical Investigation*, *129*(7), 2619–2628. https://doi.org/10.1172/JCI124615
45. Jiemy, W. F., Sleen, Y., Geest, K. S., Berge, H. A., Abdulahad, W. H., Sandovici, M., Boots, A. M., Heeringa, P., & Brouwer, E. (2020). Distinct macrophage phenotypes skewed by local granulocyte macrophage colony-stimulating factor (GM-CSF) and macrophage colony-stimulating factor (M-CSF) are associated with tissue destruction and intimal hyperplasia in giant cell arteritis. *Clinical & Translational Immunology*, *9*(9). https://doi.org/10.1002/cti2.1164
46. Jiemy, W. F. (2021). Macrophage diversity in the pathogenesis of vasculitides: implications for diagnosis and treatment *[University of Groningen]*. https://doi.org/10.33612/diss.183292913
47. Van Sleen, Y., Jiemy, W. F., Pringle, S., Geest, K. S. M., Abdulahad, W. H., Sandovici, M., Brouwer, E., Heeringa, P., & Boots, A. M. H. (2021). A Distinct Macrophage Subset Mediating Tissue Destruction and Neovascularization in Giant Cell Arteritis: Implication of the YKL-40/Interleukin-13 Receptor α2 Axis. *Arthritis & Rheumatology*. https://doi.org/10.1002/art.41887
48. Roslind, A., & Johansen, J. S. (2009). YKL-40: A Novel Marker Shared by Chronic Inflammation and Oncogenic Transformation (pp. 159–184). https://doi.org/10.1007/978-1-59745-447-6_7
49. Simm, A., Nestler, M., & Hoppe, V. (1997). PDGF-AA, a Potent Mitogen for Cardiac Fibroblasts from Adult Rats. *Journal of Molecular and Cellular Cardiology*, *29*(1), 357–368. https://doi.org/10.1006/jmcc.1996.0280
50. Kardas, G., Daszyńska-Kardas, A., Marynowski, M., Brząkalska, O., Kuna, P., & Panek, M. (2020). Role of Platelet-Derived Growth Factor (PDGF) in Asthma as an Immunoregulatory Factor Mediating Airway Remodeling and Possible Pharmacological Target. *Frontiers in Pharmacology*, *11*. https://doi.org/10.3389/fphar.2020.00047
51. Joshi, N., Watanabe, S., Verma, R., Jablonski, R. P., Chen, C.-I., Cheresh, P., Markov, N. S., Reyfman, P. A., McQuattie-Pimentel, A. C., Sichizya, L., Lu, Z., Piseaux-Aillon, R., Kirchenbuechler, D., Flozak, A. S., Gottardi, C. J., Cuda, C. M., Perlman, H., Jain, M., Kamp, D. W., … Misharin, A. v. (2020). A spatially restricted fibrotic niche in pulmonary fibrosis is sustained by M-CSF/M-CSFR signalling in monocyte-derived alveolar macrophages. *European Respiratory Journal*, *55*(1), 1900646. https://doi.org/10.1183/13993003.00646-2019
52. Preisser, L., Miot, C., Guillou-Guillemette, H., Beaumont, E., Foucher, E. D., Garo, E., Blanchard, S., Frémaux, I., Croué, A., Fouchard, I., Lunel-Fabiani, F., Boursier, J., Roingeard, P., Calès, P., Delneste, Y., & Jeannin, P. (2014). IL-34 and macrophage colony-stimulating factor are overexpressed in hepatitis C virus fibrosis and induce profibrotic macrophages that promote collagen synthesis by hepatic stellate cells. *Hepatology*, *60*(6), 1879–1890. https://doi.org/10.1002/hep.27328
53. Chen, S., So, E. C., Strome, S. E., & Zhang, X. (2015). Impact of Detachment Methods on M2 Macrophage Phenotype and Function. *Journal of Immunological Methods*, *426*, 56–61. https://doi.org/10.1016/j.jim.2015.08.001
54. Feuerer, N., Morschl, J., Daum, R., Weiss, M., Hinderer, S., Schenke-Layland, K., & Shipp, C. (2021). Macrophage retrieval from 3D biomaterials: A detailed comparison of common

dissociation methods. *Journal of Immunology and Regenerative Medicine*, *11*, 100035. https://doi.org/10.1016/j.regen.2020.100035
55. Malheiro, V., Elbs-Glatz, Y., Obarzanek-Fojt, M., Maniura-Weber, K., & Bruinink, A. (2017). Harvesting pre-polarized macrophages using thermo-responsive substrates. *Scientific Reports*, *7*(1), 42495. https://doi.org/10.1038/srep42495
56. Malorny, U., Neumann, C., & Sorg, C. (1981). Influence of Various Detachment Procedures on the Functional State of Cultured Murine Macrophages. *Immunobiology*, *159*(4–5), 327–336. https://doi.org/10.1016/S0171-2985(81)80090-3
57. Orecchioni, M., Ghosheh, Y., Pramod, A. B., & Ley, K. (2019). Macrophage Polarization: Different Gene Signatures in M1(LPS+) vs. Classically and M2(LPS–) vs. Alternatively Activated Macrophages. *Frontiers in Immunology*, *10*. https://doi.org/10.3389/fimmu.2019.01084
58. Philipp J. Hohensinner, Julia Mayer, Julia Kichbacher, Julia Kral-Pointner, Barbara Thaler, Christoph Kaun, Lena Hell, Patrick Haider, Marion Mussbacher, Johannes A. Schmid, Stefan Stojkovic, Svitlana Demyanets, Michael B. Fischer, Kurt Huber, Katharina Wöran, Christian Hengstenberg, Walter S. Speidl, Rudolf Oehler, Ingrid Pabinger, & Johann Wojta. (2020). Alternative activation of human macrophages enhances tissue factor expression and production of extracellular vesicles. *Haematologica*, *106*(2), 454–463. https://doi.org/10.3324/haematol.2019.220210
59. Puig-Kröger, A., Sierra-Filardi, E., Domínguez-Soto, A., Samaniego, R., Corcuera, M. T., Gómez-Aguado, F., Ratnam, M., Sánchez-Mateos, P., & Corbí, A. L. (2009). Folate Receptor β Is Expressed by Tumor-Associated Macrophages and Constitutes a Marker for M2 Anti-inflammatory/Regulatory Macrophages. *Cancer Research*, *69*(24), 9395–9403. https://doi.org/10.1158/0008-5472.CAN-09-2050
60. Liu, X., Yin, S., Chen, Y., Wu, Y., Zheng, W., Dong, H., Bai, Y., Qin, Y., Li, J., Feng, S., & Zhao, P. (2018). LPS-induced proinflammatory cytokine expression in human airway epithelial cells and macrophages via NF-κB, STAT3 or AP-1 activation. *Molecular Medicine Reports*. https://doi.org/10.3892/mmr.2018.8542
61. Unuvar Purcu, D., Korkmaz, A., Gunalp, S., Helvaci, D. G., Erdal, Y., Dogan, Y., Suner, A., Wingender, G., & Sag, D. (2022). Effect of stimulation time on the expression of human macrophage polarization markers. *PLOS ONE*, *17*(3), e0265196. https://doi.org/10.1371/journal.pone.0265196
62. Lefort, C. T., & Kim, M. (2010). Human T Lymphocyte Isolation, Culture and Analysis of Migration In Vitro. *Journal of Visualized Experiments*, *40*. https://doi.org/10.3791/2017
63. Eksioglu, E., Mahmood, S., Chang, M., & Reddy, V. (2007). GM-CSF promotes differentiation of human dendritic cells and T lymphocytes toward a predominantly type 1 proinflammatory response. *Experimental Hematology*, *35*(8), 1163–1171. https://doi.org/10.1016/j.exphem.2007.05.001
64. Parajuli, B., Sonobe, Y., Kawanokuchi, J., Doi, Y., Noda, M., Takeuchi, H., Mizuno, T., & Suzumura, A. (2012). GM-CSF increases LPS-induced production of proinflammatory mediators via upregulation of TLR4 and CD14 in murine microglia. *Journal of Neuroinflammation*, *9*(1), 268. https://doi.org/10.1186/1742-2094-9-268
65. Lukic, A., Larssen, P., Fauland, A., Samuelsson, B., Wheelock, C. E., Gabrielsson, S., & Radmark, O. (2017). GM-CSF– and M-CSF–primed macrophages present similar resolving but distinct inflammatory lipid mediator signatures. *The FASEB Journal*, *31*(10), 4370–4381. https://doi.org/10.1096/fj.201700319R
66. Bender, A. (2004). Differentiation of human monocytes in vitro with granulocyte–macrophage colony-stimulating factor and macrophage colony-stimulating factor produces

distinct changes in cGMP phosphodiesterase expression. *Cellular Signaling*, *16*(3), 365–374. https://doi.org/10.1016/j.cellsig.2003.08.009
67. Montagnani, S., Postiglione, L., Giordano-Lanza, G., di Meglio, F., Castaldo, C., Sciorio, S., Montuori, N., di Spigna, G., Ladogana, P., Oriente, A., & Rossi, G. (2009). Granulocyte macrophage colony stimulating factor (GM-CSF) biological actions on human dermal fibroblasts. *European Journal of Histochemistry*, *45*(3), 219. https://doi.org/10.4081/1632
68. Buranasin, P., Mizutani, K., Iwasaki, K., Pawaputanon Na Mahasarakham, C., Kido, D., Takeda, K., & Izumi, Y. (2018). High glucose-induced oxidative stress impairs proliferation and migration of human gingival fibroblasts. *PLOS ONE*, *13*(8), e0201855. https://doi.org/10.1371/journal.pone.0201855
69. Van den Bossche, J., & Saraber, D. L. (2018). Metabolic regulation of macrophages in tissues. *Cellular Immunology*, *330*, 54–59. https://doi.org/10.1016/j.cellimm.2018.01.009
70. O'Neill, L. A. J., & Pearce, E. J. (2016). Immunometabolism governs dendritic cell and macrophage function. *Journal of Experimental Medicine*, *213*(1), 15–23. https://doi.org/10.1084/jem.20151570
71. Viola, A., Munari, F., Sánchez-Rodríguez, R., Scolaro, T., & Castegna, A. (2019). The Metabolic Signature of Macrophage Responses. *Frontiers in Immunology*, *10*. https://doi.org/10.3389/fimmu.2019.01462
72. Wang, F., Zhang, S., Vuckovic, I., Jeon, R., Lerman, A., Folmes, C. D., Dzeja, P. P., & Herrmann, J. (2018). Glycolytic Stimulation Is Not a Requirement for M2 Macrophage Differentiation. *Cell Metabolism*, *28*(3), 463-475.e4. https://doi.org/10.1016/j.cmet.2018.08.012
73. Tavakoli, S., Short, J. D., Downs, K., Nguyen, H. N., Lai, Y., Zhang, W., Jerabek, P., Goins, B., Sadeghi, M. M., & Asmis, R. (2017). Differential Regulation of Macrophage Glucose Metabolism by Macrophage Colony-stimulating Factor and Granulocyte-Macrophage Colony-stimulating Factor: Implications for ^{18}F-FDG PET Imaging of Vessel Wall Inflammation. *Radiology*, *283*(1), 87–97. https://doi.org/10.1148/radiol.2016160839
74. Na, Y. R., Gu, G. J., Jung, D., Kim, Y. W., Na, J., Woo, J. S., Cho, J. Y., Youn, H., & Seok, S. H. (2016). GM-CSF Induces Inflammatory Macrophages by Regulating Glycolysis and Lipid Metabolism. *The Journal of Immunology*, *197*(10), 4101–4109. https://doi.org/10.4049/jimmunol.1600745
75. Lacey, D. C., Achuthan, A., Fleetwood, A. J., Dinh, H., Roiniotis, J., Scholz, G. M., Chang, M. W., Beckman, S. K., Cook, A. D., & Hamilton, J. A. (2012). Defining GM-CSF– and Macrophage-CSF–Dependent Macrophage Responses by In Vitro Models. *The Journal of Immunology*, *188*(11), 5752–5765. https://doi.org/10.4049/jimmunol.1103426
76. Riss, T. L., Moravec, R. A., Niles, A. L., Duellman, S., Benink, H. A., Worzella, T. J., & Minor, L. (2004). *Cell Viability Assays*.
77. Graefe, C., Eichhorn, L., Wurst, P., Kleiner, J., Heine, A., Panetas, I., Abdulla, Z., Hoeft, A., Frede, S., Kurts, C., Endl, E., & Weisheit, C. K. (2019). Optimized Ki-67 staining in murine cells: a tool to determine cell proliferation. *Molecular Biology Reports*, *46*(4), 4631–4643. https://doi.org/10.1007/s11033-019-04851-2
78. Regnard, G. & van Loosdregt, I. T. (2020). Wound healing assays: discussing subtypes of cell removal assays. *Cyto Smart*.
79. Shabestani Monfared, G., Ertl, P., & Rothbauer, M. (2020). An on-chip wound healing assay fabricated by xurography for evaluation of dermal fibroblast cell migration and wound closure. *Scientific Reports*, *10*(1), 16192. https://doi.org/10.1038/s41598-020-73055-7
80. Rodriguez-Menocal, L., Salgado, M., Ford, D., & van Badiavas, E. (2012). Stimulation of Skin and Wound Fibroblast Migration by Mesenchymal Stem Cells Derived from Normal Donors

and Chronic Wound Patients. *Stem Cells Translational Medicine*, *1*(3), 221–229. https://doi.org/10.5966/sctm.2011-0029

81. Corbera-Bellalta, M., Alba-Rovira, R., Muralidharan, S., Espígol-Frigolé, G., Ríos-Garcés, R., Marco-Hernández, J., Denuc, A., Kamberovic, F., Pérez-Galán, P., Joseph, A., D'Andrea, A., Bondensgaard, K., Cid, M. C., & Paolini, J. F. (2022). Blocking GM-CSF receptor α with mavrilimumab reduces infiltrating cells, pro-inflammatory markers and neoangiogenesis in ex vivo cultured arteries from patients with giant cell arteritis. *Annals of the Rheumatic Diseases*, *81*(4), 524–536. https://doi.org/10.1136/annrheumdis-2021-220873
82. Applications of Percoll In Blood Cells. (2022). *Merck KGaA*.
83. Liu, Y., Li, Y., Li, N., Teng, W., Wang, M., Zhang, Y., & Xiao, Z. (2016). TGF-β1 promotes scar fibroblasts proliferation and transdifferentiation via up-regulating MicroRNA-21. *Scientific Reports*, *6*(1), 32231. https://doi.org/10.1038/srep32231
84. Pakyari, M., Farrokhi, A., Maharlooei, M. K., & Ghahary, A. (2013). Critical Role of Transforming Growth Factor Beta in Different Phases of Wound Healing. *Advances in Wound Care*, *2*(5), 215–224. https://doi.org/10.1089/wound.2012.0406

7. APPENDIX

7.1. Optimization of monocyte isolation and macrophage differentiation

The goal of the monocyte isolation and MØ differentiation was to obtain a proper amount of pure and differentiated MØs per condition. This was needed, because an appropriate density of MØs in at least 500 µL culture medium was demanded during MØ activation. It was expected to need at least 500 µL culture medium (the acquired MØ culture supernatant at the end) per condition since this was used for the ELISA, MTT assay, and scratch assay. ELISA required a total of 130 µL supernatant (YKL-40, PDGF-AA, and IL-6), whereas the MTT and scratch assay needed 150 and 50 µL supernatant, respectively. This resulted in a total of 330 µL required supernatant per condition whereby the remaining 170 µL (or more) supernatant was taken into account for mistakes or further research.

To establish the optimal protocol for the aforementioned requirements, multiple experiments were performed of the monocyte isolation and MØ differentiation before executing the final batches. Firstly, monocytes were isolated from PBMCs solely based on 2 hours adherence in a 6 well plate (1 cryovial per well) followed by washing. These monocytes were subsequently differentiated into MØs over the course of 7 days whilst changing medium on day 2 and 4. Even though enough differentiated MØs were obtained for MØ activation, monocyte isolation and differentiation was further improved to increase the MØ purity, density, and amount. Secondly, monocytes were isolated from PBMCs using separation based on Percoll® gradients, which is able to isolate certain blood cells based on separation by size and density [82]. These monocytes were differentiated into MØs in a 12 well plate (1 cryovial per 2 wells) over the course of 7 days whilst changing medium on day 3 and 5. Flow cytometry (antibodies for CD14 and CD16) on the isolated monocytes showed a monocyte purity of 67% and the presence of classical (mainly), non-classical, and intermediate monocytes. Although, a monocyte purity of 67% was considered descent, it could be further improved since there were still many lymphocytes present in the culture. During differentiation into MØs, it was also observed that the monocyte density was low.

At last, to further improve both the monocyte purity and density, monocytes were isolated from PBMCs using a combination of Percoll® gradients and 4 hours adherence in a 12 well plate with 1 cryovial per well. These monocytes were similarly differentiated into MØs over the course of 7 days whilst changing medium on day 3 and 5. Overall, the addition of monocyte adherence greatly boosted the monocyte purity, because most of the non-adhering lymphocytes were washed away, whereas monocytes sticked to the plastic of the well plate. In this way, monocytes were differentiated into MØs at a good purity, density, and amount. Using this optimized protocol, a minimum of 150,000 and a maximum of 500,000 differentiated MØs were obtained per condition for the final batches. With these amounts, either 50,000 or 100,000 MØs in either 0.5 or 1 mL culture medium were used for MØ activation with (un)stimulated conditions, contributing to an appropriate ratio between MØs and supernatant.

Notably, also the differentiation into the MØ subtypes (GM/M-MØs) was confirmed over the course of 7 days. Monocytes cultured in the presence of GM-CSF differentiated into large and round GM-MØs, whereas monocytes in the presence of M-CSF differentiated into spindle-like M-MØs, showed below in Figure 9 and 10, respectively.

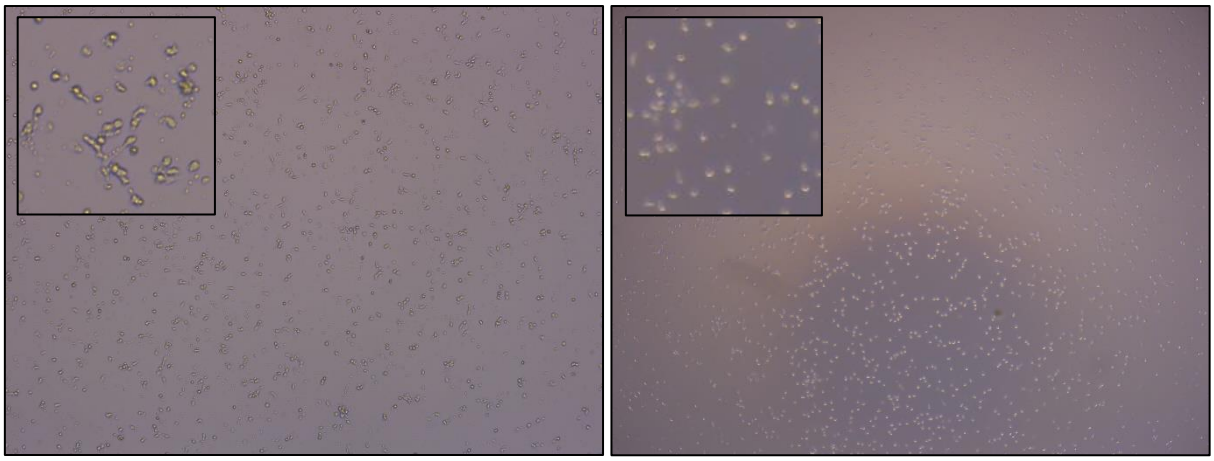

Figure 9. Monocyte differentiation into large and round GM-MØs in the presence of GM-CSF. Left culture day 0 and right culture day 7 (40x magnified along with enlarged image).

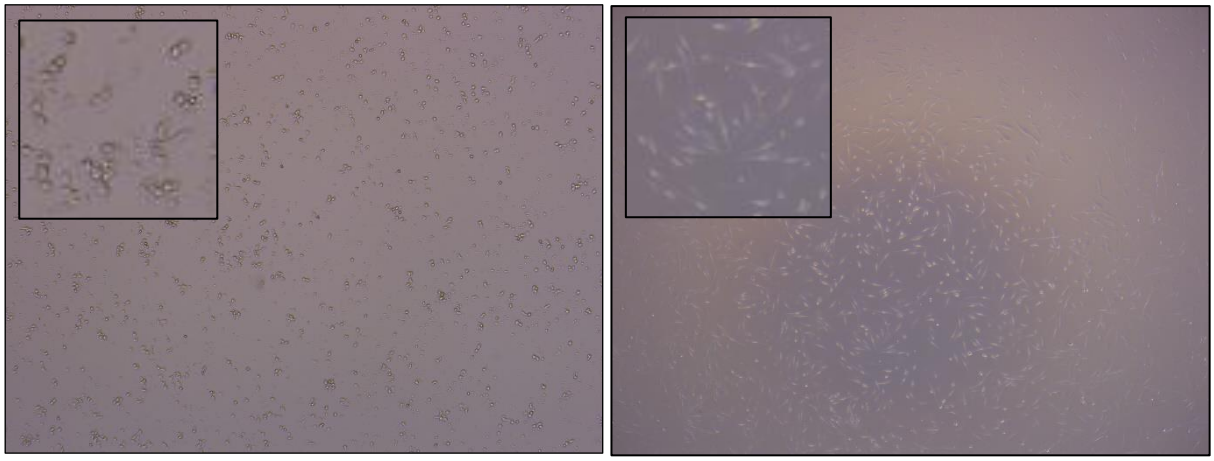

Figure 10. Monocyte differentiation into spindle-like M-MØs in the presence of M-CSF. Left culture day 0 and right culture day 7 (40x magnified along with enlarged image).

7.2. Optimization of MTT assay

The goal of the MTT assay was to assess the proliferative capacity of fibroblasts in the presence of GM/M-MØ culture supernatant. To allow further expansion of fibroblasts by proliferation, an optimal cell seeding density was needed whilst also maintaining a healthy fibroblast culture. Next to that, also external factors needed to be minimized to make sure that fibroblast proliferation was mainly due to the MØ culture supernatant. Fibroblasts were therefore cultured in low-serum growth medium for a certain time to halt proliferation before addition of the MØ culture supernatant. Moreover, to increase the sensitivity of the assay, also incubation time and concentration of MØ culture supernatant was optimized. To achieve the optimization of the aforementioned requirements, a total of 14 MTT assay pilots were performed with varying cell seeding densities, serum concentrations (low-serum growth medium), incubation time and steps, and MØ culture supernatant concentrations. For the MØ culture supernatant a practice batch from buffy 2 of conditions with (un)stimulated GM/M-MØs at 100,000 cells/mL was used.

At first, MTT assays with different cell seeding densities along with varying incubation times and steps were carried out. It was found out that the seeding density of 5,000 cells/well was best since that still allowed expansion of fibroblasts whilst also maintaining a healthy fibroblast culture. Moreover, it was observed that direct seeding in low-serum growth medium with a FCS concentration of 0.1% was sufficient for maintaining a healthy fibroblast culture. Though, it was also seen that washing at this seeding density resulted in the removal of cells specifically between the outer edge and center of the

well. This loss of cells during washing was still observed when higher serum concentrations were used for the low-serum growth medium or when cells were first incubated in regular growth medium (10% FCS). To overcome this problem, fibroblasts were directly seeded in low-serum growth medium (0.1% FCS), whereafter 24 hours, a part of the culture medium was removed and replaced with the corresponding MØ culture supernatant. In this way, fibroblast proliferation was mostly due to the MØ culture supernatant, because the initial low-serum growth medium diminished the effect of the regular growth medium on fibroblast proliferation (during general fibroblast culturing). After a certain incubation period with the MØ culture supernatant, a small amount of MTT solution was added. After incubation, culture medium was removed, which did not remove formazan crystals, whereafter MTT solvent was added.

Next, varying MØ culture supernatant concentrations and incubation times were carried out. Supernatant concentrations of 20, 40, and 50% with incubation times of 2, 3, or 4 days were tried, where it became clear that the supernatant concentration of 50% and incubation time of 3 days resulted in the most sensitive assay with the largest differences between conditions. With an incubation time of 2 days too small differences between conditions were seen, whereas for 4 days fibroblast cultures became too confluent and dead cells were seen.

Worth to mention is the variation in cell density between different MTT assay pilots. At first, fibroblasts were counted using the cell counter, which caused variations in cell density between different pilots wherein the same seeding density was used. Later, cell counting was instead performed with the hemacytometer to be more consistent. This resulted in an unexpected small increase in cell density for the final MTT assay with MØ culture supernatant from buffy 1-6. It is thought that cell counting by the cell counter resulted in a seeding density under 5,000 cells/well, whereas counting with the hemacytometer actually resulted in a seeding density of 5,000 cells/well. Though, for the final MTT assay, there was still room for further expansion of the fibroblasts in the presence of MØ culture supernatant, although limited. The cell density of <5,000 cells/well (counted with cell counter) is depicted below in Figure 11. Again, the actual cell density was unfortunately slightly higher for the final MTT assay.

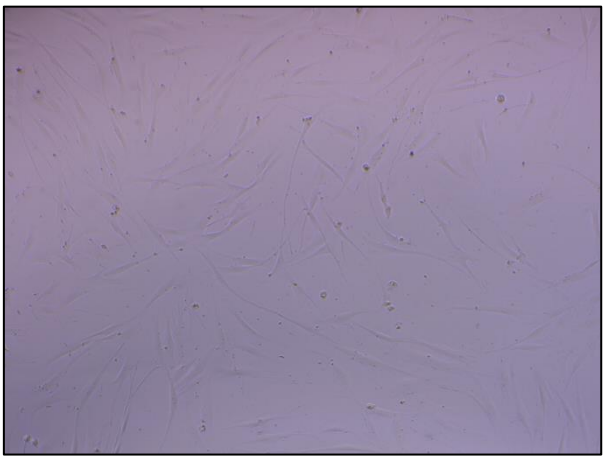

Figure 11. Fibroblast seeding density of <5,000 cells/well for the optimized MTT assay (100x magnified).

Besides, also investigation in negative and positive controls was done, so that conditions with MØ culture supernatant could be compared with a control. As a negative control, fibroblasts were cultured in solely low-serum growth medium since this had minimal effect on fibroblast proliferation. Though, it was observed that solely low-serum growth medium still resulted in a small expansion of the fibroblasts. For a positive control, TGF-β was used, because it was reported as promotor of dermal

fibroblast proliferation [83] and it was the only available GF in the lab. In a MTT assay pilot, it was observed that increasing concentrations of TGF-β (maximal 50 ng/mL) resulted in a relative increase of fibroblast proliferation, showed by higher formazan absorbances for higher TGF-β concentrations. Thus, it was decided to use the highest TGF-β concentration as a positive control for the MTT assay. Unfortunately, no negative control was added in the pilot that tested TGF-β, so no comparison could be made between the control types. Because of the variation in cell density due to the change in cell counting method, no difference was seen between the negative and positive control for the final MTT assay. It is suspected that for the assessment of the negative control, a lower seeding density was used compared to the assessment of the positive control, which resulted in the assumption that low-serum growth medium did not promote fibroblast proliferation, whereas TGF-β did. However, it became clear for the final MTT assay (with unexpected higher seeding densities) that both low-serum growth medium and TGF-β had similar effects on fibroblast proliferation, suggesting that TGF-β did not have a strong effect after all. Therefore, the negative control was used to compare the conditions with MØ culture supernatant with each other (Results 3.2).

7.3. Optimization of scratch assay

The goal of the scratch assay was to assess the migratory capacities of fibroblasts in the presence of GM/M-MØ culture supernatant. To make sure fibroblast migration was mainly due to the MØ culture supernatant and not by regular fibroblast proliferation, fibroblasts needed to be cultured in low-serum growth medium for a certain time to halt proliferation, similar to the MTT assay. Also similar to the MTT assay was the optimization of the cell seeding density. Moreover, scratch application and time of application was also assessed to further improve the consistency of the assay. As for the sensitivity of the assay, also concentration of the MØ culture supernatant was optimized. Above all, the scratch assay had to be done in a 24 well plate with 500 µL culture medium since there was a limited amount of MØ culture supernatant. To achieve the optimization of the aforementioned requirements, a total of 14 scratch assay pilots were performed with varying cell seeding densities, incubation times, scratch applications and times, and MØ culture supernatant concentrations. For the MØ culture supernatant a practice batch from buffy 2 of conditions with (un)stimulated GM/M-MØs at 100,000 cells/mL was used.

To start, scratch assays with different cell seeding densities, incubation times, and scratch application times were carried out. At first, it was concluded that a seeding density of 100,000 cells/well was the most convenient since it yielded a constant and confluent fibroblast culture without overcrowding. However, due to inconsistencies with cell counting (similar as with the MTT assay optimization), an unexpected higher cell density was observed when cells were counted with the hemacytometer. Therefore, the optimal seeding density was re-assessed wherefrom the seeding density of 50,000 cells/well came out as the most convenient. As for the incubation time, it was observed that direct seeding in low-serum growth medium (0.1% FCS) for 24 hours resulted in a healthy fibroblast culture with minimal proliferation. In this way, scratch application was best when performing it after the initial incubation in low-serum growth medium. It was most practical to perform the scratch application late in the day, so that migration could be assessed after 16 and 24 hours after scratch application (post-scratch application time points). For pilots that only included low-serum growth medium, there was still room for more migration at these post-scratch application time points. This was ideal since fibroblasts would probably migrate more during the final scratch assay that included MØ culture supernatant. The optimal cell seeding density of 50,000 cells/well before and after scratch application is depicted below in Figure 12.

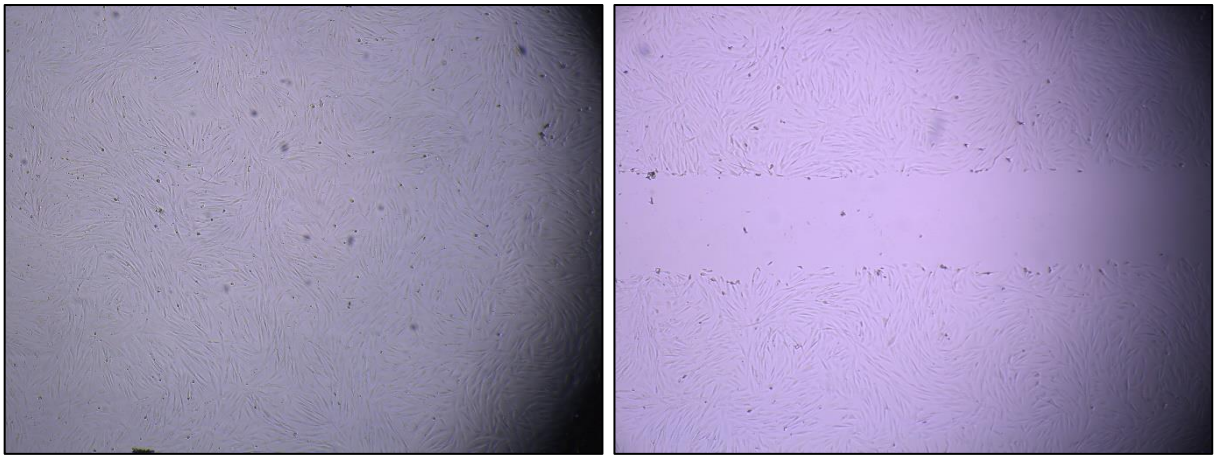

Figure 12. Fibroblast seeding density of 50,000 cells/well for the optimized scratch assay. Left pre-scratch (after 24 hours in low-serum growth medium) and right 0 hours post-scratch (40x magnified).

Thereafter, varying concentrations of MØ culture supernatant were used to see at what concentration the assay would be most sensitive at the post-scratch time points. When a supernatant concentration of 20% was used, it was observed that migration for most conditions already reached towards its maximum at 24 hours post-scratch. Though, when using a supernatant concentration of 10%, it was seen that migration averaged between minimal and maximal migration for both post-scratch time points. Thus, a 10% concentration of MØ culture supernatant was used for the final scratch assay since it would be the most sensitive to observe differences between conditions.

Additionally, negative and positive controls were assessed, so that conditions with MØ culture supernatant could be compared with a control. As a negative control, fibroblasts were cultured in solely low-serum growth medium during migration since it was suspected that low-serum growth medium had minimal influence on fibroblast migration. For the positive control, again TGF-β was used since it is established that TGF-β is an essential GF for the recruitment of fibroblasts in the wound healing process *in vivo* [84]. But as with the MTT assay, TGF-β was again the only available GF in the lab. During a scratch assay pilot, it was seen that increasing concentrations of TGF-β (maximal 50 ng/mL) did not visibly increase migration. However, due to the potency of TGF-β in wound healing, it was decided to use the highest TGF-β concentration as a positive control for the final scratch assay. Unfortunately, it became clear during the final scratch assay that TGF-β performed worser than the negative control (low-serum growth medium only). Therefore, the negative control was used to compare the conditions with MØ culture supernatant with each other (Results 3.2).

7.4. Use of TScratch

TScratch is a user friendly software tool that allows automatic analysis for scratch assays. Images were obtained as JPEG files and subsequently uploaded into the TScratch program. Images were then globally analyzed in the group editing mode followed by additional editing in the single image mode using the threshold slider (algorithm for open image area) and the paint tool. An example of the work flow is shown below in Figure 13.

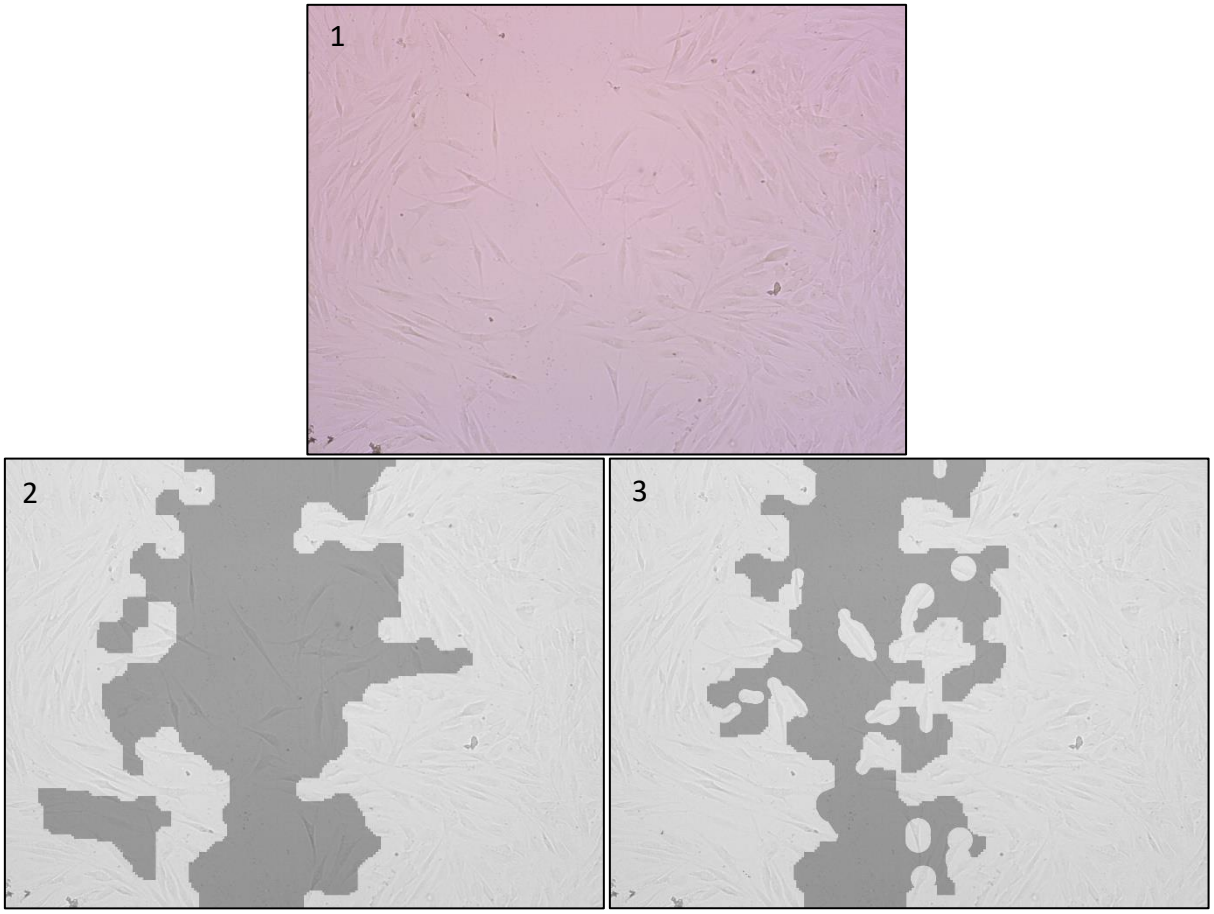

Figure 13. Work flow of TScratch analysis (images are 100x magnified). 1: Unedited image (JPEG). 2: Initial analysis in global editing mode (35.1% wound area). 3: Final analysis in single image mode using the threshold slider and the paint tool (23.9% wound area).

7.5. Distinct macrophage expression pattern due to GM/M-CSF

Next to the monocyte differentiation into GM/M-MØs from buffy 1-6 and donor 7-8, also monocyte differentiation was performed with a slightly different protocol. These experiments with an altered protocol were performed at an earlier stage of this project and in a different project by W. F. Jiemy and A. Zhang. Notably, for these altered MØ differentiations, RPMI (4.5 g/L glucose, 10% FCS and 50 ng/mL gentamycin) was used instead of DMEM (1 g/L glucose, 10% FCS, 1% penicillin-streptomycin, and 1% L-glutamine).

For the altered MØ differentiation in this project, monocytes were isolated from PBMCs of buffy 1 using only 2 hours adherence in a 6 well plate (1 cryovial per 2 wells). These monocytes were subsequently differentiated into GM/M-MØs in the presence of respectively GM/M-CSF (50 ng/mL) whilst changing medium on day 2 and 4. After 7 days, all MØs were similarly activated as with buffy 1-6 (Materials & Methods 2.3), but instead activation was performed at 50,000 cells per 1 mL. After 24 hours, MØs were lysed and supernatants were collected. With the MØ lysates, qPCR was performed on CD206, YKL-40, FR-β, and PDGF-A (Materials & Methods 2.4). The results are represented below in Figure 14. It was observed that GM-MØs show higher expression of CD206 and YKL-40 compared to M-MØs. It must be mentioned that also M-MØs had high expression of YKL-40 shown by the high relative expression to actin-β, though, there was still higher expression in GM-MØs. For M-MØs on the other hand, higher expression of FR-β and PDGF-A was observed compared to GM-MØs. To note, barely any expression of FR-β was observed in GM-MØs, whereas for PDGF-A minimal expression was

shown in both MØs subsets indicated by the very low relative expression. Together these results confirmed the model described in Introduction 1.3 and 1.4.

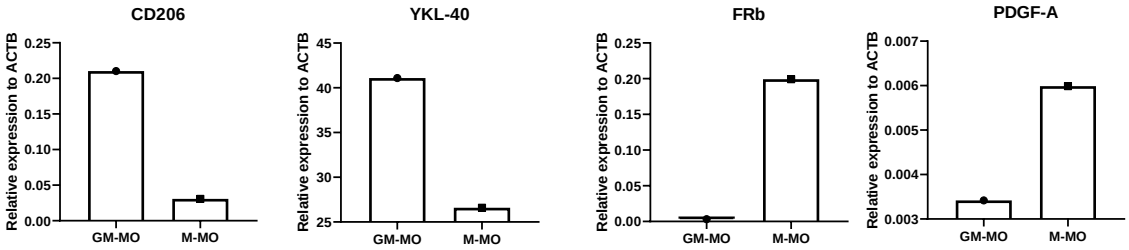

Figure 14. Differential expression of CD206, YKL-40, FR-β, and PDGF-A on skewed MØs as a result of GM/M-CSF.

For the altered MØ differentiation from a different project, monocytes were isolated from HC PBMCs by negative selection using a monocyte enrichment kit that does not deplete $CD16^+$ monocytes. These monocytes were subsequently differentiated at 500,000 cells/well (24 well plate) into GM/M-MØs at a higher 100 ng/mL GM/M-CSF concentration whilst changing medium on day 3 and 5. After 7 days, half of MØs were activated without detachment using IFN-γ, whereas the other half were not activated. After 24 hours with GM/M-CSF with or without IFN-γ, MØs were detached, counted, and lysed similarly as with buffy 1-6 (Materials & Methods 2.3). With the MØ lysates, qPCR was performed on CD206, IL-6, and FR-β (Materials & Methods 2.4). The results are represented below in Figure 15. It was observed that GM-MØs showed higher expression of CD206 (mainly with unstimulated GM-MØs) and IL-6 compared to M-MØs. In contrast, FR-β expression was mainly observed in both (un)stimulated M-MØs. Of note, it was observed that monocytes showed no expression of CD206, IL-6, and FR-β. Again, these results confirmed the model described in Introduction 1.3 and 1.4.

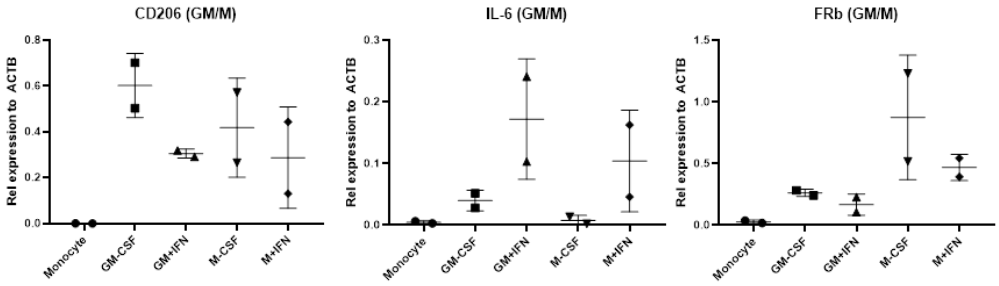

Figure 15. Differential expression of CD206, IL-6, and FR-β on skewed MØs as a result of GM/M-CSF.